

# Modeling and forecasting subnational age distribution of death counts

Han Lin Shang 

Department of Actuarial Studies and Business Analytics  
Macquarie University

Cristian F. Jiménez-Varón \*

Department of Mathematics  
University of York

## Abstract

Existing mortality forecasting methods focus on age-specific mortality rates, which lie in an unconstrained space and overlook the distributional nature of life-table death counts. Few studies have developed and compared forecasting methods that model the shape and dynamics of the age distribution of deaths, especially at the subnational level, where data quality varies greatly. This paper presents several forecasting methods to model and forecast the subnational age distribution of death counts. The age distribution of death counts has many similarities to probability density functions, which are nonnegative and have a constrained integral, and thus live in a constrained nonlinear space. To address the nonlinear nature of objects, we implement a cumulative distribution function transformation that is scale-free and has additional monotonicity. Using subnational Japanese life-table death counts from [Japanese Mortality Database \(2025\)](#), we evaluate the forecast accuracy of the transformation and forecasting methods. The improved forecast accuracy of life-table death counts implemented here will be of great interest to demographers in estimating regional age-specific survival probabilities and life expectancy, and to actuaries for determining annuity prices for various ages and maturities.

**Keywords:** conformal prediction intervals; constrained functional time series; cumulative distribution function transformation; life-table death counts; principal component analysis

---

\*Corresponding postal address: Department of Mathematics, Heslington, York YO10 5DD, United Kingdom; Email: cristian.jimenezvaron@york.ac.uk

# 1 Introduction

Accurate prediction of subnational mortality rates plays a crucial role in both actuarial studies and demographic planning. From a demographic perspective, subnational mortality forecasts inform regional health planning, pension sustainability assessments, and population projections that guide policy decisions on healthcare infrastructure and resource allocation (see, e.g., [Booth and Tickle, 2008](#)). In actuarial science, understanding spatial variations in mortality and their evolution over time is essential for pricing life insurance products, designing annuities, and managing longevity risk in pension schemes (e.g., [Cairns et al., 2006](#); [Haberman and Renshaw, 2011](#)). Subnational mortality prediction allows actuaries and policymakers to capture heterogeneity across regions, reflecting socioeconomic, environmental, and healthcare disparities, improving the reliability of longevity projections ([Li and Lee, 2005](#)).

Although there exist many multipopulation techniques, such as the [Li and Lee's \(2005\)](#) method, for modeling and forecasting age-specific mortality rates, the age distribution of death counts is another mortality instrument, which possesses its unique advantages over mortality rates. For example, the age distribution of death counts preserves distributional information: the age distribution of deaths retains the shape of how deaths are spread across ages. Due to non-negativity and summability, the changes are relative in age. It captures shifts in longevity more directly: the mode and spread of the distribution can be measured. It is less sensitive to population size estimates; at the subnational level, these estimates may be unreliable. Although mortality rates at older ages can be outside their plausible range  $(0,1)$ , it does not occur for the age distribution of death counts. It facilitates comparison across populations and time, as it is insensitive to population size estimates. The age distribution of death counts is an explicit way of measuring the probability of dying, commonly studied in the [Cairns et al.'s \(2006\)](#) model.

Following the early works of [Lu et al. \(2020 and 2021\)](#) on subnational mortality rates and [Bergeron-Boucher et al. \(2018\)](#) on subnational age distribution of death counts, we present several forecasting methods to model and predict the subnational age distribution of deaths, which are also useful for applications in actuarial science, such as fixed-term or lifetime annuity pricing (see, e.g., [Shang and Haberman, 2020](#)). Apart from subnational age distributions of deaths in demography ([Jiménez-Varón et al., 2025](#)), density-valued objects for multiple groups are common, with examples including income distributions across different populations ([Kneip and Utikal, 2001](#)), financial return distributions for multiple stocks ([Petersen et al., 2022](#)), distributions of

bidding times in online auctions for various items (Wang et al., 2008), among others.

Since age distributions of deaths naturally take the form of density functions, they are well-suited for modeling using advanced forecasting techniques from compositional and functional data analyses. Oeppen (2008) demonstrates that the use of compositional data analysis to forecast the age distribution of death counts performs similarly in accuracy to forecast age-specific mortality rates. Within compositional data analysis, the Lee-Carter model is frequently applied to model and forecast unconstrained data. Shang and Haberman (2020) extend this approach by incorporating a functional data-analytic perspective, including multiple principal components and nonparametric smoothing. Recently, Shang and Haberman (2025b) introduce a cumulative distribution function (CDF) transformation, converting each year's age distribution of deaths into a probability bounded within the unit interval to address the presence of zero values. Through cumulative summation, a probability density function can be transformed into a CDF, providing the additional benefit of monotonicity (see also Mayhew and Smith, 2013). With a time series of CDFs, it is common to model and extrapolate the pattern using a logistic transformation.

Multiple density-valued objects observed over time are related to high-dimensional functional time series (HDFTS). In the statistical literature, Zhou and Dette (2023) derive Gaussian and multiplier bootstrap approximations for the sums of HDFTS. With these approximations, they construct joint simultaneous confidence bands for the mean functions and develop a hypothesis to test whether the mean functions in the cross-sectional dimension exhibit parallel behavior. Hallin et al. (2023) investigate the representation of HDFTS using a factor model and determine conditions on the eigenvalues of the covariance operator that are crucial for establishing the existence and uniqueness of the factor model. Gao et al. (2019) adopt a two-stage approach, combining truncated principal component analysis and a separate scalar factor model for the resulting panels of scores. Tavakoli et al. (2023) introduce a functional factor model with a functional factor loading and a vector of real-valued factors, while Guo et al. (2025) propose a functional factor model with a real-valued factor loading and a functional factor. Leng et al. (2026) introduce a unified framework that accommodates both types of factor models. Tang et al. (2022) study clustering for age-specific subnational mortality rates, which is an example of HDFTS. Li et al. (2024) introduce hypothesis tests and estimation procedures for testing and locating (common) change points. Chang et al. (2025) develop a two-stage procedure for modeling and forecasting HDFTS.

Although numerous studies have addressed the modelling and forecasting of age distributions of death counts at the national level (see, e.g., Shang, 2025; Shang and Haberman, 2025a and b),

there remains a notable gap in extending such forecasts to the subnational level. Our contributions are twofold. First, we present several visualization techniques to capture patterns in the age distribution of death counts and to display contrasts between subnational and national data. Second, we revisit several forecasting methods and compare their point and interval forecast accuracy with applications to subnational life-table death counts. For different sexes and prefectures, we provide some recommendations on the optimal multipopulation models, which can vary in terms of their point and interval forecast accuracies. The improvement in forecast accuracy of life-table death counts may translate to more accurate annuity prices and life expectancy calculations; in turn, these inform policymakers on the sustainability of the pension system and aged care facilities.

Our paper is structured as follows. In Section 2, we describe our motivating data set and introduce a series of image plots for displaying important features in HDFTS. In Section 3, we present the CDF transformations. Within the CDF transformation, we consider a number of forecasting methods in Section 4 to model and forecast unconstrained functional time-series data. In Section 5, we propose two general strategies for constructing pointwise prediction intervals for the age distribution of death counts. In Section 6, we evaluate and compare point forecast accuracy using the Kullback-Leibler divergence (KLD) and Jensen-Shannon divergence (JSD), and interval forecast accuracy using the coverage probability difference (CPD) and mean interval score. In Section 6.6, we show relationship between life-table death count and survival probability and life expectancy. In Section 6.7, we present a model diagnostic analysis using functional analysis of variance. Section 7 concludes with ideas on how the methodology presented can be extended.

## 2 Subnational age distribution of death in Japan

In many developed countries, such as Japan, increases in longevity and an aging population have led to concerns about the sustainability of pension, health, and aged care systems (see, e.g., [Coulmas, 2007](#)). These concerns have led to a surge of interest among government policymakers in accurately modeling and forecasting age-specific mortality. Subnational forecasts of age-specific mortality are useful for informing policy at the local level, and any improvement in forecast accuracy is beneficial for allocating current and future resources at national and subnational levels.

In demography, the age distribution of deaths provides important insights into longevity and lifespan variability that cannot be grasped directly from the central mortality rate or survival function. As pointed out by [Oeppen \(2008\)](#), the age distribution of death counts is more suitable

than central mortality rates for computing life expectancy and annuity premia. In addition to providing an informative description of the mortality experience of a population, life-table death counts yield readily available information on the “central longevity indicators” (e.g., mean, median, and modal age at death, see [Cheung et al., 2005](#); [Canudas-Romo, 2010](#)) and lifespan variability (e.g., [van Raalte and Caswell, 2013](#); [Aburto and van Raalte, 2018](#)). The life-table death count is less sensitive to population size estimate, especially at the subnational level; population size estimate may be unreliable. Because of this, it is insensitive to population size estimates, which facilitates comparisons across populations and over time. The life-table death count is directly linked to the probability of dying  $q_x$ , which is the mortality instrument in the [Cairns et al.’s \(2006\)](#) model.

We study Japanese life-table death counts from 1975 to 2023, obtained from the [Japanese Mortality Database \(2025\)](#). We observe complete life-table death counts for ages from 0 to 109 in single years of age, with the last age group being age 110+. A distinctive advantage of life-table death counts lies in the availability of data observed across all ages.

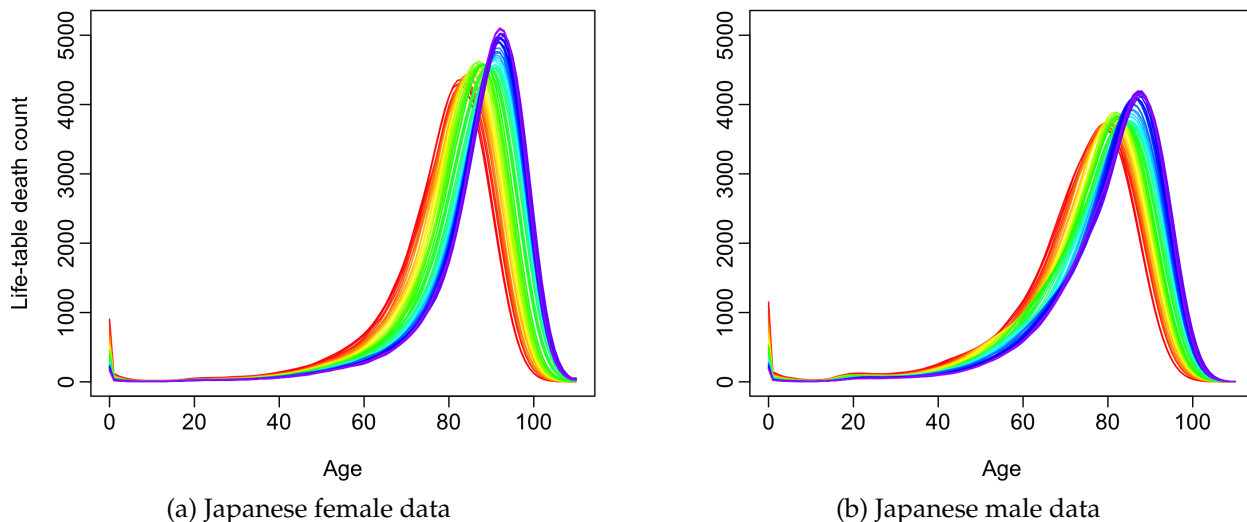


Figure 1: Functional time series graphical displays of age-specific life-table death counts from 1975 to 2023 in a single-year group. The oldest years are shown in red, with the most recent years in violet. Curves are ordered chronologically according to the colors of the rainbow.

Figure 1 shows rainbow plots of the female and male age-specific life-table death counts in Japan from 1975 to 2023. The time ordering of the curves follows the color order of a rainbow, where curves from the distant past are shown in red, and the more recent curves are shown in violet. The figures show typical mortality curves for a developed country, with a declining trend in infant mortality. A typical negatively skewed distribution of life-table death counts is apparent,

with the peaks shifting to higher ages for both females and males. This shift is a major source of longevity risk, which is a major issue for insurers and pension funds, especially in the sale and risk management of annuity products (see [Denuit et al., 2007](#), for a discussion). In addition, the spread of the distribution indicates the variability in lifespan. A decrease in variability over time can be directly observed and quantified using the Gini coefficient ([Wilmoth and Horiuchi, 1999](#); [Debón et al., 2017](#)).

In [Figure 2](#), we present a map of 47 Japanese prefectures from the northern region, Hokkaido, to the southern region, Okinawa. Due to geography and socio-economic status, the age distributions of death counts tend to be heterogeneous. Differences between prefectures or years within the same prefecture can be visualized using image plots in [Section 2.1](#) and quantified using the functional cross-correlation function in [Section 2.2](#).



Figure 2: A geographical map of 47 prefectures in Japan.

## 2.1 Image plots

Another visual perspective of the data is shown in the image plot of [Figure 3](#). To measure the distance between two probability densities, such as the subnational and national age distributions of death counts, we consider the symmetric KLD (see [Edwards and Tuljapurkar, 2005](#); [d’Albis et al., 2014](#), for examples of using the KLD to compare country-specific lifespan distributions). For

a given prefecture and gender, the symmetric KLD can be expressed as

$$\begin{aligned} \text{KLD}_s^g &= D_{\text{KL}} [d_{t,s}^g(\mathbf{u})|d_{t,\text{national}}^g(\mathbf{u})] + D_{\text{KL}} [d_{t,\text{national}}^g(\mathbf{u})|d_{t,s}^g(\mathbf{u})] \\ &= \frac{1}{111 \times n} \sum_{t=1}^n \sum_{i=1}^{111} d_{t,s}^g(\mathbf{u}_i) \times [\ln d_{t,s}^g(\mathbf{u}_i) - \ln d_{t,\text{national}}^g(\mathbf{u}_i)] + \\ &\quad \frac{1}{111 \times n} \sum_{t=1}^n \sum_{i=1}^{111} d_{t,\text{national}}^g(\mathbf{u}_i) \times [\ln d_{t,\text{national}}^g(\mathbf{u}_i) - \ln d_{t,s}^g(\mathbf{u}_i)], \end{aligned}$$

where  $n$  denotes the number of years in the data set. Here, we graph the symmetric KLD between life-table death counts for each prefecture to life-table death counts for the whole country, thus allowing relative mortality comparisons to be made.

A divergent color palette is used, with red representing larger KLD values (i.e., greater difference between subnational and national data) and yellow denoting smaller KLD values. The prefectures are ordered geographically from north to south, so the most northerly prefecture (Hokkaido) is at the top of the panels, and the most southerly prefecture (Okinawa) is at the bottom.

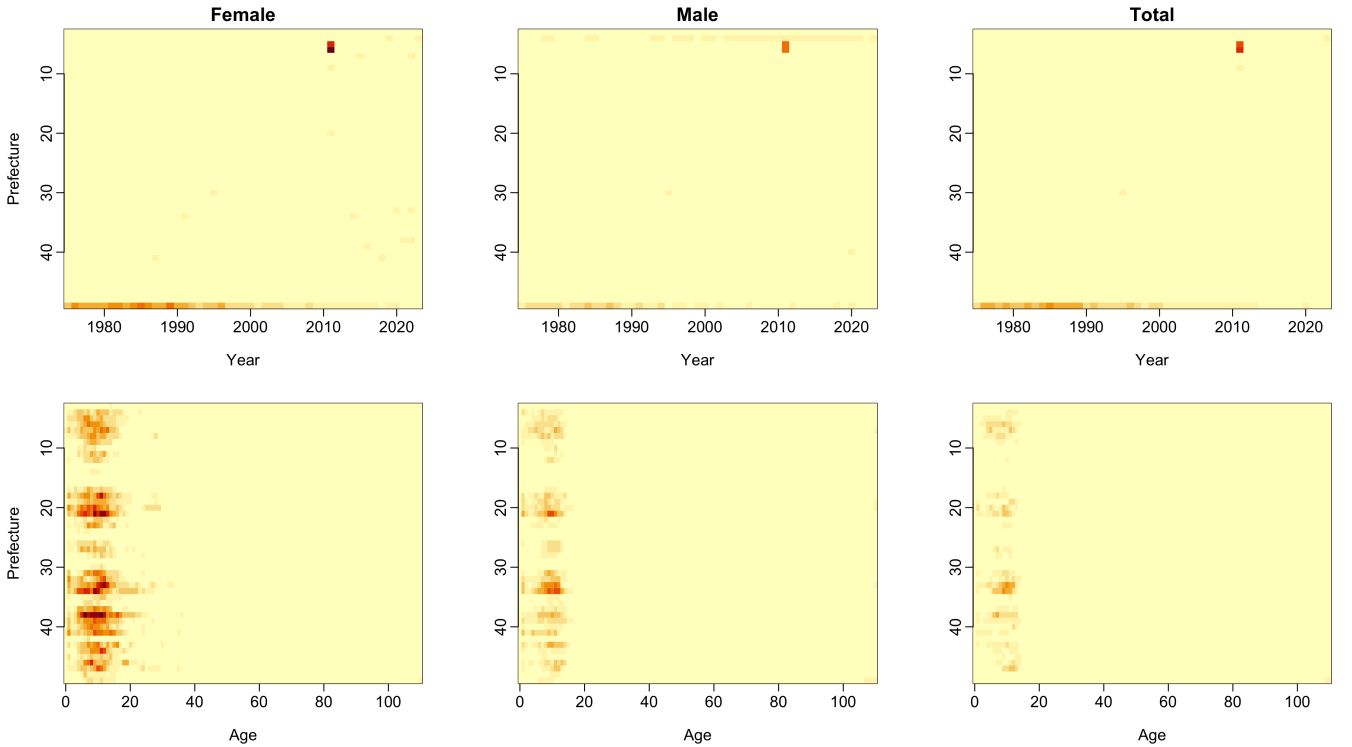


Figure 3: Image plots showing the symmetric KLD between life-table death counts of a prefecture and life-table death counts of the whole country. The top panel shows mortality averaged over ages, while the bottom panel shows mortality averaged over years. Prefectures are numbered geographically from north to south.

The top row of the panels shows mortality for each prefecture and year, averaged over all ages. In 2011, in Iwate, Miyagi, and Fukushima, there was a large increase in mortality compared to other prefectures. These are northern coastal regions, and the elevated relative mortality is due to the tsunami of 11 March 2011 (see, e.g., [Nakahara and Ichikawa, 2013](#)) caused by a magnitude-9.0 earthquake.

In 1995, there was an increase in mortality for Hyogo, which corresponds to the Kobe (Great Hanshin) earthquake (magnitude 6.9) of 17 January 1995. Also evident is the mortality difference in Okinawa up to 2000, suggesting a decline in the relative mortality advantages enjoyed by residents in this region.

The bottom of the panels shows the mortality for each prefecture and age, averaged over all years. Several striking features are apparent. There are differences between prefectures in the care of children and adolescents; this may be due to socio-economic differences and the accessibility of health services ([Tanaka et al., 2023](#); [Okamoto et al., 2025](#)).

## 2.2 Functional cross-correlation plot

Let  $d_{t,s}^g(u)$  be the age distribution of deaths for age  $u$ , prefecture  $s$ , gender  $g$  at year  $t$ , respectively. There are 111 ages,  $S = 47$  prefectures, and 49 years. Following [Kokoszka et al. \(2017\)](#) and [Mestre et al. \(2021\)](#), the functional autocorrelation coefficient at lag  $h$  can be defined as

$$\begin{aligned} \|C_h\| &= \iint C_h^2(u, u) du du \\ \rho_h &= \frac{\|C_h\|}{\int C_0(u, u) du}, \end{aligned} \quad (1)$$

where  $h$  denotes a lag and  $C_h(u, u) = \text{cov}[d_{t,s}^g(u), d_{t+h,s}^g(u)]$ . The functional cross-covariance at lag  $h$  can be expressed as

$$\|C_h[d_s^g(u), d_{\text{national}}^g(v)]\| = \iint C_h^2[d_s^g(u), d_{\text{national}}^g(v)] du dv,$$

where  $C_h[d_s^g(u), d_{\text{national}}^g(v)] = \text{cov}[d_{t,s}^g(u), d_{t+h,\text{national}}^g(v)]$ . The functional cross-correlation at lag  $h$  is then given by

$$\rho_h[d_s^g(u), d_{\text{national}}^g(v)] = \frac{\|C_h[d_s^g(u), d_{\text{national}}^g(v)]\|}{\sqrt{\int C_0[d_s^g(u), d_s^g(u)] du} \sqrt{\int C_0[d_{\text{national}}^g(v), d_{\text{national}}^g(v)] dv}}. \quad (2)$$

When  $d_s^g(\mathbf{u}) = d_{\text{national}}^g(\mathbf{v})$ , cross correlation in (2) reduces to autocorrelation in (1).

In Figure 4, we display the functional cross-correlation functions showing the dependence of life-table death counts between each prefecture and the whole country. Each subnational data set shows a stronger cross-correlation with the national data at lags 1 and 2. The cross-correlation reduces as lag increases.

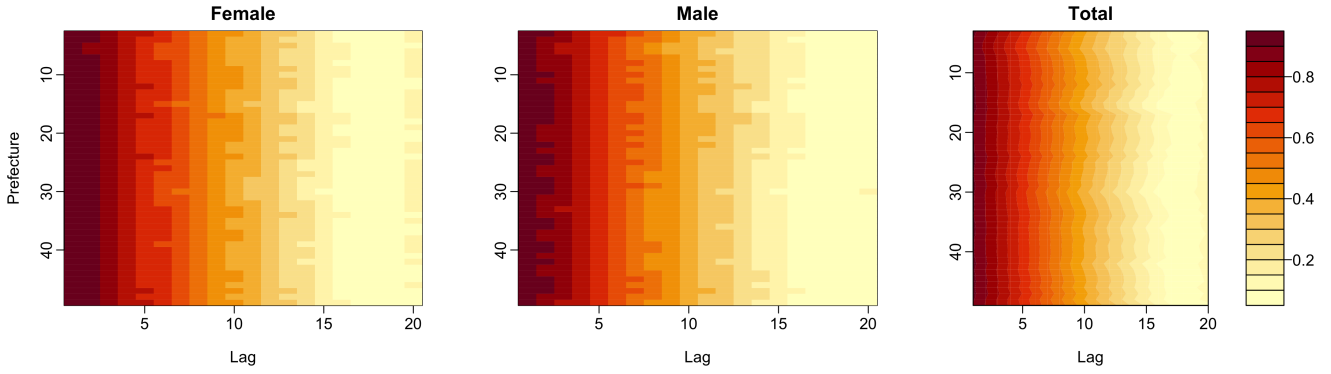


Figure 4: Functional cross-correlation plots showing the dependence of the female, male, and total life-table death counts between each prefecture and the whole country. Prefectures are numbered geographically from north to south.

### 3 Cumulative distribution function transformation

To model life-table death counts, there exists a range of transformations, including centered log-ratio transformation (Aitchison, 1986),  $\alpha$ -transformation (Shang and Haberman, 2025c), and CDF transformation (Shang and Haberman, 2025b). Among the three, the CDF transformation can handle not only zero counts but also the monotonicity constraint. In the CDF transformation, we first convert an age distribution of death for each year to a probability by dividing its radix  $10^5$ . Via the cumulative sum, we transform a probability density function into a CDF,

$$D_{t,s}^g(\mathbf{u}_x) = \sum_{i=1}^x d_{t,s}^g(\mathbf{u}_i), \quad x = 1, \dots, 111, \quad t = 1, \dots, n,$$

where  $D_{t,s}^g(\mathbf{u}_{111}) = 1$ . In doing so, it enjoys the additional benefit of monotonicity (see also Mayhew and Smith, 2013).

Then, we perform a logistic transformation,

$$\mathcal{X}_{t,s}^g(\mathbf{u}_x) = \text{logit}[D_{t,s}^g(\mathbf{u}_x)] = \ln \left[ \frac{D_{t,s}^g(\mathbf{u}_x)}{1 - D_{t,s}^g(\mathbf{u}_x)} \right],$$

where  $\ln(\cdot)$  denotes the natural logarithm. Since  $D_{t,s}^g(\mathbf{u}_{111}) = 1$ , the last column is removed to avoid the undefinedness of the logistic transformation. By considering age as a continuum, the object  $\mathcal{X}_{t,s}^g(\mathbf{u})$  is an example of a high-dimensional functional time series.

To transform  $\mathcal{X}_{t,s}^g(\mathbf{u}_x)$  back to the original scale, we first perform an inverse logit transformation, obtaining

$$D_{t,s}^g(\mathbf{u}_x) = \frac{\exp^{\mathcal{X}_{t,s}^g(\mathbf{u}_x)}}{1 + \exp^{\mathcal{X}_{t,s}^g(\mathbf{u}_x)'}}$$

where we add back the last column of ones. Then, we take the first-order differencing to obtain

$$d_{t,s}^g(\mathbf{u}_x) = \Delta_{i=1}^x D_{t,s}^g(\mathbf{u}_i) \times 10^5,$$

where  $\Delta$  represents the first-order differencing, where  $\Delta_{i=1}^1 D_{t,s}^g(\mathbf{u}_1) = D_{t,s}^g(\mathbf{u}_1)$ . The constant  $10^5$  is the radix of the life-table death count. Since the data are observed discretely, we use cumulative sums and first-order differences to approximate integration and differentiation, respectively.

## 4 Functional time-series forecasting models

We obtain a set of unconstrained functional time series  $(\mathcal{X}_{1,s}^g(\mathbf{u}), \dots, \mathcal{X}_{n,s}^g(\mathbf{u}))$  via the CDF transformation. Generally, we represent it as  $\{\mathcal{X}_{t,s}^g(\mathbf{u})\}$ , which is an arbitrary functional time series defined in a common probability space. It is assumed that the observations  $\mathcal{X}_{t,s}^g(\mathbf{u})$  are elements of the Hilbert space  $\mathcal{H} = \mathcal{L}^2(\mathcal{J})$  equipped with the inner product  $\langle w, v \rangle = \int_{\mathcal{J}} w(\mathbf{u})v(\mathbf{u})d\mathbf{u}$ , where  $\mathbf{u}$  represents a continuum and  $\mathcal{J} \subset \mathbb{R}$  denotes a function support range and  $\mathbb{R}$  is the real line. Each function is a square-integrable function that satisfies  $\|\mathcal{X}_{t,s}^g\|^2 = \int_{\mathcal{J}} (\mathcal{X}_{t,s}^g(\mathbf{u}))^2 d\mathbf{u} < \infty$  and the associated norms.

### 4.1 Univariate functional time-series (UFTS) forecasting method

We assume  $\mathcal{X}_{t,s}^g(\mathbf{u})$  has a finite mean and variance. Then, its non-negative definite covariance function is given by

$$\begin{aligned} c_s^g(\mathbf{u}, \mathbf{v}) &:= \text{Cov}[\mathcal{X}_s^g(\mathbf{u}), \mathcal{X}_s^g(\mathbf{v})] \\ &= \text{E}\{[\mathcal{X}_s^g(\mathbf{u}) - \mu_s^g(\mathbf{u})][\mathcal{X}_s^g(\mathbf{v}) - \mu_s^g(\mathbf{v})]\}, \quad \forall \mathbf{u}, \mathbf{v} \in \mathcal{J}, \end{aligned}$$

where  $\mu_s^g(\mathbf{u}) = \mathbb{E}\{\mathcal{X}_{t,s}^g(\mathbf{u})\}$ . By Mercer's lemma, there exists a set of orthonormal sequences  $(\phi_k)$  of continuous functions in  $\mathcal{L}^2(\mathcal{J})$  and a non-increasing sequence  $\lambda_{k,s}^g$  of positive numbers such that

$$c_s^g(\mathbf{u}, \mathbf{v}) = \sum_{k=1}^{\infty} \lambda_{k,s}^g \phi_{k,s}^g(\mathbf{u}) \phi_{k,s}^g(\mathbf{v}),$$

where  $\lambda_{k,s}^g$  and  $\phi_{k,s}^g(\mathbf{u})$  denote the  $k^{\text{th}}$  eigenvalue and eigenfunction, respectively. The Karhunen-Loève expansion of a stochastic process  $\mathcal{X}_{t,s}^g(\mathbf{u})$  can be expressed as

$$\begin{aligned} \mathcal{X}_{t,s}^g(\mathbf{u}) &= \mu_s^g(\mathbf{u}) + \sum_{k=1}^{\infty} \beta_{t,k,s}^g \phi_{k,s}^g(\mathbf{u}) \\ &= \mu_s^g(\mathbf{u}) + \sum_{k=1}^{K_s^g} \beta_{t,k,s}^g \phi_{k,s}^g(\mathbf{u}) + e_{t,s}^g(\mathbf{u}), \end{aligned}$$

where the principal component score  $\beta_{t,k,s}^g$  is given by the projection of  $[\mathcal{X}_{t,s}^g(\mathbf{u}) - \mu_s^g(\mathbf{u})]$  in the direction of the  $k^{\text{th}}$  eigenfunction  $\phi_{k,s}^g(\mathbf{u})$ , i.e.,  $\beta_{t,k,s}^g = \langle \mathcal{X}_{t,s}^g(\mathbf{u}) - \mu_s^g(\mathbf{u}), \phi_{k,s}^g(\mathbf{u}) \rangle$ ; and  $e_{t,s}^g(\mathbf{u})$  denotes the model error function with a mean of zero and a finite variance, and  $K_s^g < n$  is the number of retained components. The eigenfunctions represent the fixed shapes of variation (e.g., longevity shift), while the scores capture the time-varying magnitude of these shifts.

There are a number of ways to select the retained number of principal components, such as the bootstrap approach proposed by [Hall and Vial \(2006\)](#) and [Bathia et al. \(2010\)](#), description length approach proposed by [Poskitt and Sengarapillai \(2013\)](#), pseudo-Akaike information criterion ([Shibata, 1981](#)), scree plot ([Cattell, 1966](#)), and eigenvector variability plot ([Tu et al., 2009](#)). We consider the eigenvalue ratio criterion (EVR) of [Li et al. \(2020\)](#), defined as

$$K_s^g = \arg \min_{k=1, \dots, K_{\max}} \left\{ \frac{\widehat{\lambda}_{k+1,s}^g}{\widehat{\lambda}_{k,s}^g} \times \mathbb{1} \left\{ \frac{\widehat{\lambda}_{k,s}^g}{\widehat{\lambda}_{1,s}^g} \geq \eta \right\} + \mathbb{1} \left\{ \frac{\widehat{\lambda}_{k,s}^g}{\widehat{\lambda}_{1,s}^g} < \eta \right\} \right\}, \quad (3)$$

where  $\mathbb{1}\{\cdot\}$  is the binary indicator function,  $\eta = \frac{1}{\ln[\max(\widehat{\lambda}_{1,s}^g, n)]}$  is a small positive value. Instead of searching through  $n$ , we restrict our searching range by setting  $k_{\max} = \#\{k | \widehat{\lambda}_{k,s}^g \geq \frac{1}{n} \sum_{k=1}^n \widehat{\lambda}_{k,s}^g, k \geq 1\}$ . For comparison, we also consider  $K_s^g = 6$  as suggested in [Hyndman et al. \(2013\)](#). Note that when  $K_s^g = 1$ , it reduces to the [Lee and Carter's \(1992\)](#) model.

Conditioning on the observed functions  $\mathcal{X}_s^g(\mathbf{u}) = [\mathcal{X}_{1,s}^g(\mathbf{u}), \dots, \mathcal{X}_{n,s}^g(\mathbf{u})]$  and the estimated functional principal components  $\mathbf{B} = \{\phi_{1,s}^g(\mathbf{u}), \dots, \phi_{K_s^g,s}^g(\mathbf{u})\}$ , the  $h$ -step-ahead point forecast of

$\mathcal{X}_{n+h,s}^g(\mathbf{u})$  can be expressed as

$$\widehat{\mathcal{X}}_{n+h|n,s}^g(\mathbf{u}) = \mathbb{E}[\mathcal{X}_{n+h,s}^g(\mathbf{u}) | \mathcal{X}_s^g(\mathbf{u}), \mathbf{B}] = \widehat{\boldsymbol{\mu}}_s^g(\mathbf{u}) + \sum_{k=1}^{K_s^g} \widehat{\boldsymbol{\beta}}_{n+h|n,k,s}^g \widehat{\Phi}_{k,s}^g(\mathbf{u}),$$

where  $\widehat{\boldsymbol{\mu}}_s^g(\mathbf{u}) = \frac{1}{n} \sum_{t=1}^n \mathcal{X}_{t,s}^g(\mathbf{u})$  and  $\widehat{\boldsymbol{\beta}}_{n+h|n,k,s}^g$  denotes time-series forecasts of the  $k^{\text{th}}$  principal component scores. The forecasts of these scores can be obtained via a univariate time-series forecasting method, such as exponential smoothing (Hyndman et al., 2008). Computationally, we implement the `ets` function in the forecast package (Hyndman and Khandakar, 2008), which selects the optimal parameters based on the corrected Akaike information criterion.

## 4.2 Multivariate functional time-series (MFTS) forecasting method

The univariate functional time-series method does not account for correlations between female and male data within the same region. However, explicitly modeling the correlation between multiple series may improve forecast accuracy. We consider a multivariate functional time-series method to jointly model and forecast multiple series that may be correlated.

Let  $\mathcal{X}_{t,s}^F(\mathbf{u})$  and  $\mathcal{X}_{t,s}^M(\mathbf{u})$  represent female and male subnational age distribution of death counts. As our multiple functional time series have the same function support, we consider data where each observation consists of  $\omega \geq 2$  functions, that is,  $[\mathcal{X}_{t,s}^F(\mathbf{u}), \mathcal{X}_{t,s}^M(\mathbf{u})] \in \mathbb{R}^2$ , where  $\mathbf{u} \in \mathcal{J}$ .

Multivariate functional time series are stacked into a vector. Let  $\boldsymbol{\nu}_s^F(\mathbf{u})$  and  $\boldsymbol{\nu}_s^M(\mathbf{u})$  represent the mean function, respectively. For  $\mathbf{u}, \mathbf{v} \in \mathcal{J}$ , the theoretical cross-covariance function can be defined with elements

$$c_s(\mathbf{u}, \mathbf{v}) := \text{Cov}[\mathcal{X}_s^F(\mathbf{u}), \mathcal{X}_s^M(\mathbf{v})] = \mathbb{E} \{ [\mathcal{X}_s^F(\mathbf{u}) - \boldsymbol{\nu}_s^F(\mathbf{u})][\mathcal{X}_s^M(\mathbf{v}) - \boldsymbol{\nu}_s^M(\mathbf{v})] \}.$$

The Karhunen-Loève expansion of a stochastic process can be expressed as

$$\mathcal{X}_s(\mathbf{u}) = \boldsymbol{\nu}_s(\mathbf{u}) + \boldsymbol{\Phi}_s(\mathbf{u})\boldsymbol{\beta}_{t,s}^\top,$$

where  $\mathcal{X}_s(\mathbf{u}) = [\mathcal{X}_s^F(\mathbf{u}), \mathcal{X}_s^M(\mathbf{u})]$ ,  $\mathcal{X}_s^F(\mathbf{u}) = [\mathcal{X}_{1,s}^F(\mathbf{u}), \dots, \mathcal{X}_{n,s}^F(\mathbf{u})]$  denote stacked historical functions, and  $\boldsymbol{\nu}_s(\mathbf{u}) = [\boldsymbol{\nu}_s^F(\mathbf{u}), \boldsymbol{\nu}_s^M(\mathbf{u})]$ . Moreover,  $\boldsymbol{\beta}_s = (\boldsymbol{\beta}_{1,s}, \dots, \boldsymbol{\beta}_{K,s})$  and  $\boldsymbol{\beta}_{1,s} = (\beta_{1,1,s}, \dots, \beta_{n,1,s})$  are the

vectors of the principal component scores, and

$$\boldsymbol{\Phi}_s(\mathbf{u}) = \begin{bmatrix} \phi_{1,s}^F(\mathbf{u}) & \cdots & \phi_{K,s}^F(\mathbf{u}) & \cdots & \\ & & & & \\ & & & \phi_{1,s}^M(\mathbf{u}) & \cdots & \phi_{K,s}^M(\mathbf{u}) \end{bmatrix}_{2 \times (K \times 2)},$$

where  $K$  denotes the retained number of principal components shared by females and males.

Conditioning on the previous functions  $\mathcal{X}_s(\mathbf{u})$  and the estimated functional principal components  $\boldsymbol{\Phi}_s(\mathbf{u})$ , the  $h$ -step-ahead point forecast of  $\mathcal{X}_{n+h,s}(\mathbf{u})$  can be expressed as

$$\widehat{\mathcal{X}}_{n+h|n,s}(\mathbf{u}) = \text{E}[\mathcal{X}_{n+h,s}(\mathbf{u}) | \mathcal{X}_s(\mathbf{u}), \boldsymbol{\Phi}_s(\mathbf{u})] = \widehat{\nu}_s(\mathbf{u}) + \widehat{\boldsymbol{\Phi}}_s(\mathbf{u}) \widehat{\boldsymbol{\beta}}_{n+h|n,s}^\top,$$

where  $\widehat{\boldsymbol{\beta}}_{n+h|n,s}$  denotes the time-series forecasts of the principal component scores corresponding to the female and male series,  $\widehat{\nu}_s(\mathbf{u})$  and  $\widehat{\boldsymbol{\Phi}}_s(\mathbf{u})$  denote the estimated mean function and estimated functional principal components, respectively.

### 4.3 Multilevel functional time-series (MLFTS) forecasting method

The multilevel functional data model strongly resembles the two-way functional analysis of variance studied by [Morris and Carroll \(2006\)](#) and [Cuesta-Albertos and Febrero-Bande \(2010\)](#). The basic idea is to extract common patterns shared by multiple series  $R_{t,s}(\mathbf{u})$  and series-specific patterns  $U_{t,s}^g(\mathbf{u})$ . The common trend and series-specific trend are modeled by projecting them onto the eigenvectors of the covariance functions of the aggregated and series-specific stochastic processes, respectively. For  $t = 1, \dots, n$ , a curve can be expressed as

$$\mathcal{X}_{t,s}^g(\mathbf{u}) = \mu_s^g(\mathbf{u}) + R_{t,s}^c(\mathbf{u}) + U_{t,s}^g(\mathbf{u}), \quad (4)$$

where  $R_{t,s}^c(\mathbf{u})$  can be the simple average of the female and male series. To ensure model and parameter identifiability, we implement a two-stage estimation procedure based on functional principal component decomposition.

Since the stochastic processes  $R_{t,s}^c(\mathbf{u})$  and  $U_{t,s}^g(\mathbf{u})$  are unknown in practice, the population eigenvalues and eigenfunctions can only be approximated at best through a set of realizations  $\mathbf{R}_s^c(\mathbf{u})$  and  $\mathbf{U}_s^g(\mathbf{u})$ . From the covariance function of  $\mathbf{R}_s^c(\mathbf{u})$ , we can extract a set of functional principal components and their associated scores, along with a set of residual functions. From the covariance

function of the residuals, we can then extract a second set of functional principal components and their associated scores. While the first functional principal component decomposition captures the common pattern across multiple series, the second functional principal component decomposition captures the series-specific residual trend.

The sample versions of the series-specific mean function, a common trend, and the series-specific residual trend for a set of functional time series can be estimated by

$$\widehat{\mu}_s^g(\mathbf{u}) = \frac{1}{n} \sum_{t=1}^n \mathcal{X}_{t,s}^g(\mathbf{u}) \quad (5)$$

$$\mathbf{R}_{t,s}^c(\mathbf{u}) \approx \sum_{k=1}^K \beta_{t,k,s}^c \phi_{k,s}^c(\mathbf{u}) \quad (6)$$

$$\mathbf{U}_{t,s}^g(\mathbf{u}) \approx \sum_{l=1}^L \gamma_{t,l,s}^g \psi_{l,s}^g(\mathbf{u}), \quad (7)$$

where  $\widehat{\mu}_s^g(\mathbf{u})$  represents the simple average of the female or male series,  $\beta_{k,s}^c = (\beta_{1,k,s}^c, \dots, \beta_{n,k,s}^c)$  represents the  $k^{\text{th}}$  sample principal component scores of  $\mathbf{R}_s^c(\mathbf{u})$ , and  $\gamma_{l,s}^g = (\gamma_{1,l,s}^g, \dots, \gamma_{n,l,s}^g)$  represents the  $l^{\text{th}}$  sample principal component scores of  $\mathbf{U}_s^g(\mathbf{u})$ .

Plugging (5) into (7) into (4), we obtain

$$\mathcal{X}_{t,s}^g(\mathbf{u}) \approx \widehat{\mu}_s^g(\mathbf{u}) + \sum_{k=1}^K \beta_{t,k,s}^c \phi_{k,s}^c(\mathbf{u}) + \sum_{l=1}^L \gamma_{t,l,s}^g \psi_{l,s}^g(\mathbf{u}) + \mathbf{e}_{t,s}^g(\mathbf{u}),$$

where  $\mathbf{e}_{t,s}^g(\mathbf{u})$  denotes measurement error with a finite variance.

To select the retained number of components, we use the eigenvalue ratio criterion in (3). A feature of the multilevel method is its ability to estimate the proportion of variability explained by aggregated data. For a given population  $g$ , a measure of the within-cluster variability is given by

$$\frac{\sum_{k=1}^K \widehat{\lambda}_{k,s}^c}{\sum_{k=1}^K \widehat{\lambda}_{k,s}^c + \sum_{l=1}^L \widehat{\lambda}_{l,s}^g}.$$

When the common trend explains the primary mode of total variability, the within-cluster variability is close to 1.

Conditioning on observed data  $\mathcal{X}_s^g(\mathbf{u})$  and basis functions  $\Phi_s(\mathbf{u})$  and  $\Psi_s^g(\mathbf{u}) = \{\widehat{\psi}_{1,s}^g(\mathbf{u}), \dots, \widehat{\psi}_{L,s}^g(\mathbf{u})\}$ ,

the h-step-ahead forecasts can be obtained by

$$\begin{aligned}\widehat{\mathcal{X}}_{n+h|n,s}^g(\mathbf{u}) &= \mathbb{E}[\mathcal{X}_{n+h,s}^g(\mathbf{u}) | \mu_s^g(\mathbf{u}), \mathbf{X}_s^g(\mathbf{u}), \boldsymbol{\Phi}_s(\mathbf{u}), \boldsymbol{\Psi}_s^g(\mathbf{u})] \\ &= \widehat{\mu}_s^g(\mathbf{u}) + \sum_{k=1}^K \widehat{\beta}_{n+h|n,k,s}^c \widehat{\phi}_{k,s}^c(\mathbf{u}) + \sum_{l=1}^L \widehat{\gamma}_{n+h|n,l,s}^g \widehat{\psi}_{l,s}^g(\mathbf{u}),\end{aligned}$$

where  $\widehat{\mu}_s^g(\mathbf{u}) = \frac{1}{n} \sum_{t=1}^n \mathcal{X}_{t,s}^g(\mathbf{u})$ ,  $\{\widehat{\beta}_{n+h|n,k,s}^c, k = 1, \dots, K\}$  and  $\{\widehat{\gamma}_{n+h|n,l,s}^g, l = 1, \dots, L\}$  are the forecasted principal component scores, obtained from a univariate time-series forecasting method.

#### 4.4 Two-way functional analysis of variance (FANOVA)

To model  $\mathcal{X}_{t,s}^g(\mathbf{u})$ , we consider a two-way FANOVA decomposition, expressed as:

$$\mathcal{X}_{t,s}^g(\mathbf{u}) = \mu(\mathbf{u}) + \alpha_s(\mathbf{u}) + \beta^g(\mathbf{u}) + \epsilon_{t,s}^g(\mathbf{u}),$$

where  $\mu(\mathbf{u})$  denotes the functional grand effect,  $\alpha_s(\mathbf{u})$  denotes the functional row effect,  $\beta^g(\mathbf{u})$  denotes the functional column effect, and  $\epsilon_{t,s}^g(\mathbf{u})$  denotes the error function.

The FANOVA model can be estimated by means with

$$\begin{aligned}\widehat{\mu}(\mathbf{u}) &= \frac{1}{n_s \times 2 \times n} \sum_{s=1}^{n_s} \sum_{g=1}^2 \sum_{t=1}^n \mathcal{X}_{t,s}^g(\mathbf{u}) \\ \widehat{\alpha}_s(\mathbf{u}) &= \frac{1}{2 \times n} \sum_{g=1}^2 \sum_{t=1}^n \mathcal{X}_{t,s}^g(\mathbf{u}) - \widehat{\mu}(\mathbf{u}) \\ \widehat{\beta}^g(\mathbf{u}) &= \frac{1}{n_s \times n} \sum_{s=1}^{n_s} \sum_{t=1}^n \mathcal{X}_{t,s}^g(\mathbf{u}) - \widehat{\mu}(\mathbf{u}).\end{aligned}$$

Some identifiability constraints exist,  $\forall \mathbf{u} \in \mathcal{J}$ ,  $\sum_{s=1}^{n_s} \alpha_s(\mathbf{u}) = \sum_{g=1}^2 \beta^g(\mathbf{u}) = 0$ , and  $\sum_{s=1}^{n_s} \mathcal{X}_{t,s}^g(\mathbf{u}) = \sum_{g=1}^2 \mathcal{X}_{t,s}^g(\mathbf{u}) = 0$ ,  $\forall t$ . The FANOVA model decomposes the functional time series (FTS) jointly for all prefectures and genders into three parameters: the overall mean  $\widehat{\mu}(\mathbf{u})$ , which represents the *grand effect* measuring the overall baseline age distribution of deaths;  $\widehat{\alpha}_s(\mathbf{u})$ , which represents the *functional prefecture effect* measuring the time-invariant functional difference attribute to each prefecture, relative to the grand mean; and  $\widehat{\beta}^g(\mathbf{u})$ , which represents the *functional gender effect* measuring the time-invariant functional difference between genders, relative to the grand mean.

The residual functions  $\widehat{\epsilon}_{t,s}^g(\mathbf{u}) = \mathcal{X}_{t,s}^g(\mathbf{u}) - \widehat{\mu}(\mathbf{u}) - \widehat{\alpha}_s(\mathbf{u}) - \widehat{\beta}^g(\mathbf{u})$  are time-varying, for  $t = 1, \dots, n$ .

Following the methodology of [Jiménez-Varón et al. \(2024\)](#), we model and forecast these residual functions using the multivariate functional time series (MFTS) approach.

## 4.5 Two-stage functional principal component analyses

[Gao et al. \(2019\)](#) propose a two-stage functional principal component decomposition to model and forecast HDFTS. One of the earliest methods for comparison (see, e.g., [Tavakoli et al., 2023](#); [Shang, 2025](#)), it consists of three parts.

- 1) Functional principal component analysis is performed separately on each set of functional time series, resulting in  $P$  sets of principal component scores of low dimension  $p_0$ .
- 2) The first functional principal component scores from each of  $P$  sets of functional time series are combined into an  $P \times 1$  vector. We fit factor models to the scores to further reduce the dimension into an  $r \times 1$  vector, where  $r \ll P$ . The same is carried out for the second, third, and so on until the  $p_0^{\text{th}}$  scores. The vector of the  $P$  functional time series is reduced to an  $r \times p_0$  matrix consisting of factors.
- 3) A univariate time series model can be fitted to each factor, and forecasts are generated. Forecast factors can be used to construct forecast functions.

## 5 Construction of prediction intervals

We split the data sample consisting of 49 years from 1975 to 2023 into a training set consisting of 16 years, a validation set consisting of 16 years, and a testing set consisting of 17 years. While the choice of different data splits is arbitrary, it is customary in forecasting to allocate at least one-third of the total data for evaluation ([Hyndman and Athanasopoulos, 2021](#)).

Using the data in the training sample, we implement an expanding-window forecast scheme to obtain  $h$ -step-ahead density forecasts in the validation set for  $h = 1, 2, \dots, 16$ . For each horizon, we have a different number of curves in the validation set. For instance, when  $h = 1$ , we have 16 years to evaluate the forecast errors, denoted by  $\hat{\epsilon}_{m,s}^g(\mathbf{u}) = d_{m,s}^g(\mathbf{u}) - \hat{d}_{m,s}^g(\mathbf{u})$  for  $m = 1, 2, \dots, M = 16$ ; when  $h = 16$ , we have two years to evaluate the residual functions between the samples in the validation set and their corresponding forecasts. From these residual functions, we compute the

functional standard deviation, denoted by

$$\gamma(\mathbf{u}) = \text{sd}[\widehat{\epsilon}_{1,s}^g(\mathbf{u}), \dots, \widehat{\epsilon}_{M,s}^g(\mathbf{u})]. \quad (8)$$

We aim to determine  $(\bar{\xi}_\alpha, \underline{\xi}_\alpha)$  such that  $\alpha \times 100\%$  of the residuals satisfy

$$-\underline{\xi}_\alpha \gamma(\mathbf{u}) \leq \widehat{\epsilon}_{m,s}^g(\mathbf{u}) \leq \bar{\xi}_\alpha \gamma(\mathbf{u}),$$

where  $(\bar{\xi}_\alpha, \underline{\xi}_\alpha)$  are the tuning parameters.

Typically, the constants  $\bar{\xi}_\alpha$  and  $\underline{\xi}_\alpha$  are chosen equal. By the law of large numbers, one may achieve

$$\Pr \left[ -\xi_\alpha \gamma(\mathbf{u}) \leq d_{n+h,s}^g(\mathbf{u}) - \widehat{d}_{n+h,s}^g(\mathbf{u}) \leq \xi_\alpha \gamma(\mathbf{u}) \right] \approx \frac{1}{M} \sum_{m=1}^M \mathbb{1} \left[ -\xi_\alpha \gamma(\mathbf{u}) \leq \widehat{\epsilon}_{m,s}^g(\mathbf{u}) \leq \xi_\alpha \gamma(\mathbf{u}) \right],$$

where  $M$  denotes the number of years in the validation set.

To determine the optimal  $\xi_\alpha$ , the samples in the validation set are used to calibrate the prediction intervals so that the empirical coverage probabilities defined in (10) are close to their nominal coverage probabilities.

In Appendix C, we also present the conformal prediction interval approach of [Shafer and Vovk \(2008\)](#), which does not require a tuning parameter. By considering a quantile of the absolute residual functions, the pointwise prediction interval for the out-of-sample testing set is centered on the point forecast, with its spread determined by the chosen quantile.

## 6 Results

### 6.1 Expanding window scheme

An expanding window analysis of a time-series model is commonly used to assess model and parameter stability and prediction accuracy over time. The expanding window analysis assesses the stability of a model's parameters by computing parameter estimates and their forecasts over an expanding window across the sample (for details, see [Zivot and Wang, 2006](#), pp. 313–314).

Using the first 32 years from 1975 to 2006 in the Japanese subnational age- and sex-specific life-

table death counts, we produce one- to 16-step-ahead forecasts. Through an expanding-window approach, we re-estimate the parameters in the time-series forecasting models using the first 33 years from 1975 to 2007. Forecasts from the estimated models are then produced for one- to 16-step-ahead forecasts. We iterate this process by increasing the sample size by one year until reaching the end of the data period in 2023. This process produces 16 one-step-ahead forecasts, 15 two-step-ahead forecasts,  $\dots$ , and one 16-step-ahead forecast. We compare these forecasts with holdout samples to assess out-of-sample forecast accuracy. In Figure 5, we display a diagram of the expanding window forecast scheme for the forecast horizon  $h = 1$ , although we also consider other forecast horizons from  $h = 2$  to 16.

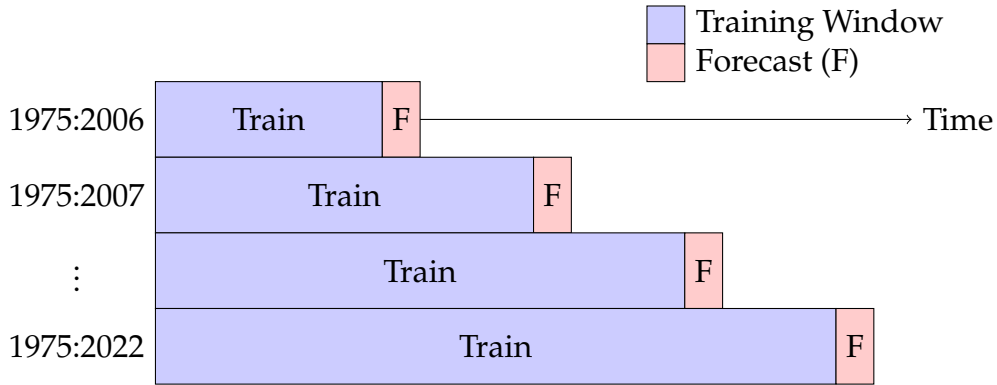


Figure 5: A diagram of the expanding-window forecast scheme.

## 6.2 Point forecast error metrics

Since life-table death counts can be considered probability density functions, we use some density-evaluation measures. These measures include the discrete version of the KLD (Kullback and Leibler, 1951), the square root of the JSD (Shannon, 1948). For two probability density functions, denoted by  $d_{m+\xi}$  and  $\hat{d}_{m+\xi}$ , the symmetric version of the KLD, also known as Jeffrey divergence, is defined as

$$\begin{aligned}
 \text{KLD}(h) &= D_{\text{KL}}(d_{m+\xi} \parallel \hat{d}_{m+\xi}) + D_{\text{KL}}(\hat{d}_{m+\xi} \parallel d_{m+\xi}) \\
 &= \frac{1}{111 \times (17 - h)} \sum_{\xi=h}^{16} \sum_{x=1}^{111} d_{m+\xi}(u_x) \cdot \left[ \ln d_{m+\xi}(u_x) - \ln \hat{d}_{m+\xi}(u_x) \right] + \\
 &\quad \frac{1}{111 \times (17 - h)} \sum_{\xi=h}^{16} \sum_{x=1}^{111} \hat{d}_{m+\xi}(u_x) \cdot \left[ \ln \hat{d}_{m+\xi}(u_x) - \ln d_{m+\xi}(u_x) \right], \quad (9)
 \end{aligned}$$

which is non-negative, for  $h = 1, 2, \dots, 16$ .

An alternative metric is the JSD, defined by

$$\text{JSD}(h) = \frac{1}{2} D_{\text{KL}}(d_{m+\xi} \| \delta_{m+\xi}) + \frac{1}{2} D_{\text{KL}}(\hat{d}_{m+\xi} \| \delta_{m+\xi}),$$

where  $\delta_{m+\xi}$  measures a common quantity between  $d_{m+\xi}$  and  $\hat{d}_{m+\xi}$ . Following the early work of [Shang and Haberman \(2020\)](#), we consider the geometric mean  $\delta_{m+\xi} = \sqrt{d_{m+\xi} \hat{d}_{m+\xi}}$ . To make the JSD a metric between two probability densities, we take the square root of the JSD (see, e.g., [Fuglede and Topsoe, 2004](#)).

### 6.3 Comparison of point forecast accuracy

In [Table 1](#), we compare the point forecast accuracy across the functional time-series models, averaged across 47 prefectures. Based on the summary statistics of the KLD and JSD, the HDFPCA model provides the most accurate point forecasts for the female data. This result indicates that the two-stage principal component analyses can adequately summarize the main features in the female data without much loss of information. The female data are relatively stable in comparison to the male counterpart. For the male data, the MFTS and MLFTS models provide the most accurate point forecasts. For the UFTS, MFTS, MLFTS, and FANOVA models, the number of retained functional principal components was determined by the EVR criterion. For the HDFPCA model, we follow the default setting of [Gao et al. \(2019\)](#), where the number of retained components is six and two in the first and second stages, respectively. In [Appendix A](#), we also provide the results for  $K = 6$  as a sensitivity analysis.

Table 1: Averaged across 47 prefectures, we evaluate and compare the point forecast accuracy of the functional time-series models, measured by the KLD and JSD. The number of components is determined by the EVR criterion.

Metric	h	Female					Male				
		UFTS	MFTS	MLFTS	FANOVA	HDFPCA	UFTS	MFTS	MLFTS	FANOVA	HDFPCA
KLD	1	0.004	0.010	0.004	0.006	0.007	0.004	0.004	0.003	0.005	0.003
	2	0.007	0.013	0.006	0.007	0.007	0.005	0.006	0.005	0.005	0.003
	3	0.008	0.015	0.007	0.009	0.009	0.006	0.007	0.005	0.006	0.004
	4	0.010	0.017	0.009	0.010	0.006	0.006	0.007	0.006	0.007	0.005

Continued on next page

Metric	h	Female					Male				
		UFTS	MFTS	MLFTS	FANOVA	HDFPCA	UFTS	MFTS	MLFTS	FANOVA	HDFPCA
	5	0.013	0.019	0.010	0.012	0.013	0.007	0.008	0.007	0.007	0.006
	6	0.015	0.021	0.011	0.013	0.007	0.008	0.009	0.007	0.008	0.007
	7	0.018	0.023	0.012	0.015	0.019	0.009	0.010	0.008	0.008	0.009
	8	0.022	0.025	0.014	0.018	0.008	0.010	0.011	0.009	0.009	0.012
	9	0.027	0.027	0.017	0.022	0.025	0.011	0.012	0.010	0.010	0.015
	10	0.033	0.030	0.021	0.026	0.010	0.012	0.014	0.011	0.011	0.018
	11	0.040	0.034	0.024	0.033	0.032	0.012	0.015	0.012	0.012	0.022
	12	0.048	0.039	0.030	0.040	0.014	0.013	0.017	0.014	0.013	0.026
	13	0.059	0.047	0.036	0.047	0.039	0.014	0.020	0.015	0.014	0.030
	14	0.068	0.040	0.042	0.061	0.019	0.014	0.012	0.015	0.017	0.035
	15	0.089	0.054	0.060	0.080	0.044	0.015	0.015	0.021	0.022	0.039
	16	0.118	0.070	0.079	0.106	0.019	0.015	0.019	0.029	0.030	0.040
	17	0.154	0.084	0.093	0.120	0.038	0.015	0.020	0.034	0.034	0.039
	Mean	0.043	0.033	0.028	0.037	0.019	0.010	0.012	0.012	0.013	0.019
	Median	0.027	0.027	0.017	0.022	0.014	0.011	0.012	0.010	0.010	0.015
JSD	1	0.034	0.049	0.034	0.039	0.042	0.030	0.032	0.028	0.034	0.029
	2	0.041	0.055	0.040	0.043	0.038	0.035	0.036	0.033	0.036	0.030
	3	0.045	0.059	0.043	0.046	0.050	0.037	0.039	0.036	0.038	0.032
	4	0.049	0.063	0.046	0.049	0.037	0.040	0.041	0.038	0.040	0.035
	5	0.054	0.066	0.049	0.053	0.060	0.042	0.043	0.040	0.041	0.039
	6	0.058	0.069	0.052	0.056	0.040	0.044	0.045	0.041	0.043	0.043
	7	0.063	0.071	0.055	0.060	0.070	0.047	0.047	0.043	0.044	0.049
	8	0.069	0.073	0.059	0.065	0.044	0.050	0.049	0.045	0.046	0.055
	9	0.076	0.075	0.063	0.070	0.082	0.052	0.051	0.048	0.047	0.062
	10	0.083	0.079	0.069	0.076	0.051	0.054	0.053	0.050	0.049	0.069
	11	0.092	0.083	0.075	0.085	0.092	0.056	0.054	0.052	0.052	0.075
	12	0.102	0.088	0.082	0.096	0.058	0.058	0.056	0.055	0.054	0.081
	13	0.116	0.094	0.092	0.106	0.100	0.060	0.059	0.058	0.057	0.087
	14	0.128	0.097	0.102	0.121	0.066	0.061	0.057	0.061	0.064	0.094
	15	0.150	0.112	0.122	0.141	0.104	0.062	0.062	0.070	0.072	0.097
	16	0.176	0.126	0.141	0.164	0.068	0.064	0.067	0.081	0.084	0.095
	17	0.202	0.134	0.152	0.175	0.094	0.064	0.069	0.087	0.088	0.093
	Mean	0.090	0.082	0.075	0.085	0.064	0.050	0.051	0.051	0.052	0.063
	Median	0.076	0.075	0.063	0.070	0.060	0.052	0.051	0.048	0.047	0.062

Figure 6 presents two heatmaps comparing seven functional time-series models across 16 forecast horizons for both female and male data. For each horizon, we count how often each method produces the smallest point forecast errors, as measured by the KLD. Choosing  $K = 6$  has a slight advantage compared to the one based on the EVR criterion. For shorter forecast horizons, the UFTS, MFTS, and MLFTS models perform equally well for the female data. However, for relatively longer forecast horizons, the HDFPCA model is recommended. For male data, the MLFTS model is generally preferred; only at the shorter forecast horizon is  $K = 6$  advantageous. For relatively longer forecast horizons, the FANOVA with the EVR criterion is recommended.

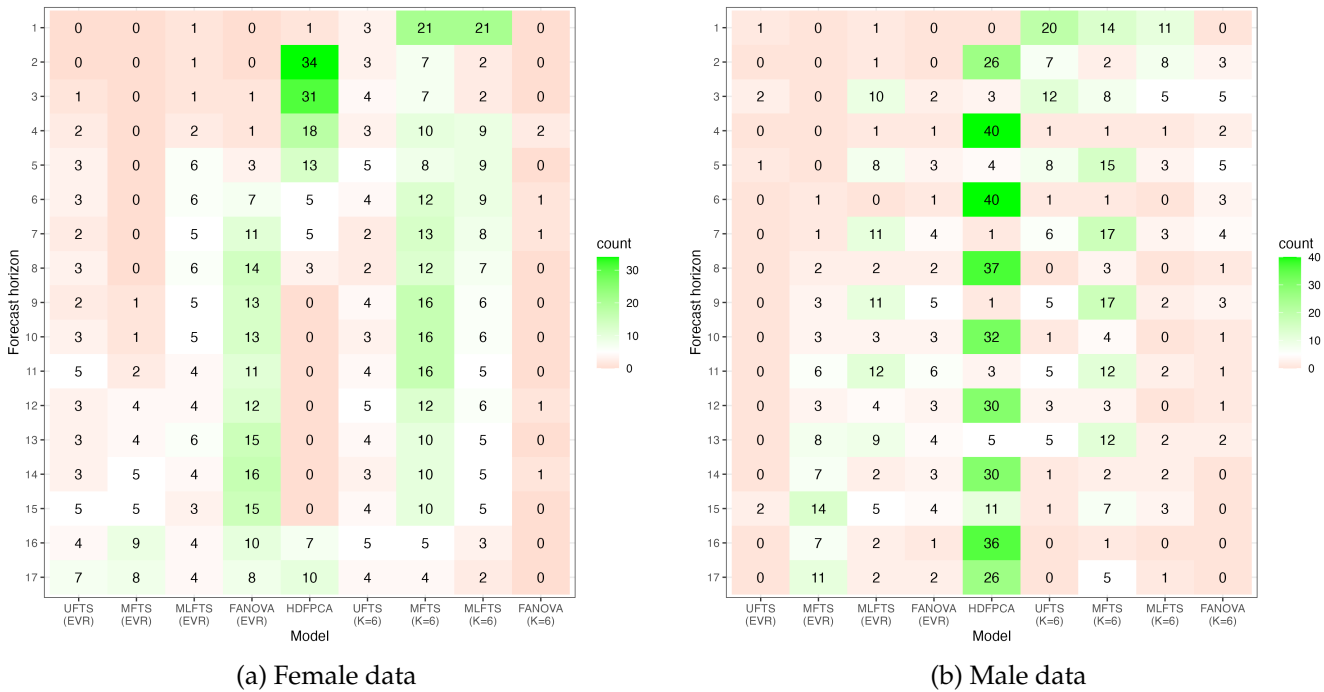


Figure 6: Heatmaps comparing the point forecast accuracy, measured by the KLD, across 17 forecast horizons for nine functional time-series models on the testing female and male data. Since there are 47 prefectures, each row sums to 47. A method that appears more than 5 times is highlighted in green, while those that appear fewer than 5 times are shown in red. If a method appears exactly five times, it is displayed in white.

To formally assess whether the observed differences in point forecast accuracy obtained via the different presented methods are statistically significant, we further apply the Model Confidence Set (MCS) procedure (Hansen et al., 2011) based on the Kullback–Leibler divergence across all forecast horizons and prefectures. The detailed MCS results and corresponding heatmap visualizations are reported in Appendix D.

## 6.4 Interval forecast error metrics

To evaluate interval forecast accuracy, we consider the CPD between the empirical coverage probability (ECP) and nominal coverage probability, as well as the mean interval score of [Gneiting and Raftery \(2007\)](#). For each year in the forecasting period, the  $h$ -step-ahead prediction intervals are computed at the  $100(1 - \alpha)\%$  nominal coverage probability. We consider the common case of the symmetric  $100(1 - \alpha)\%$  prediction intervals, with lower and upper bounds that are quantiles at  $\alpha/2$  and  $1 - \alpha/2$ , denoted by  $\widehat{d}_{n+\xi,s}^{g,lb}(\mathbf{u})$  and  $\widehat{d}_{n+\xi,s}^{g,ub}(\mathbf{u})$ . The ECP and CPD are defined as

$$\begin{aligned} \text{ECP}_h &= \frac{1}{111 \times (17 - h)} \times \sum_{\xi=h}^{16} \sum_{\mathbf{u}=1}^{111} \mathbb{1} \left\{ \widehat{d}_{\nu+\xi,s}^{g,lb}(\mathbf{u}) \leq d_{\nu+\xi,s}^g(\mathbf{u}) \leq \widehat{d}_{\nu+\xi,s}^{g,ub}(\mathbf{u}) \right\}, \\ \text{CPD}_h &= \frac{1}{111 \times (17 - h)} \times \sum_{\xi=h}^{16} \sum_{\mathbf{u}=1}^{111} \left[ \mathbb{1} \{ d_{\nu+\xi,s}^g(\mathbf{u}) > \widehat{d}_{\nu+\xi,s}^{g,ub}(\mathbf{u}) \} + \mathbb{1} \{ d_{\nu+\xi,s}^g(\mathbf{u}) < \widehat{d}_{\nu+\xi,s}^{g,lb}(\mathbf{u}) \} \right], \end{aligned} \quad (10)$$

where  $h = 1, \dots, 16$ ,  $\nu$  denotes the end of the training set when we calibrate the CPD or interval score, and  $\nu$  denotes the end of the validation set when we evaluate the interval forecast accuracy.

For different ages and years in the testing set, the mean and median CPD are defined as

$$\begin{aligned} \overline{\text{CPD}} &= \frac{1}{16} \sum_{h=1}^{16} \text{CPD}_h, \\ \text{M}[\text{CPD}] &= \text{median}(\text{CPD}_h). \end{aligned}$$

As defined by [Gneiting and Raftery \(2007\)](#), a scoring rule for the prediction intervals at age  $u$  is

$$\begin{aligned} S_{\alpha,\xi} \left[ \widehat{d}_{\nu+\xi,s}^{g,lb}(\mathbf{u}), \widehat{d}_{\nu+\xi,s}^{g,ub}(\mathbf{u}), d_{\nu+\xi,s}^g(\mathbf{u}) \right] &= \left[ \widehat{d}_{\nu+\xi,s}^{g,ub}(\mathbf{u}) - \widehat{d}_{\nu+\xi,s}^{g,lb}(\mathbf{u}) \right] \\ &+ \frac{2}{\alpha} \left[ \widehat{d}_{\nu+\xi,s}^{g,lb}(\mathbf{u}) - d_{\nu+\xi,s}^g(\mathbf{u}) \right] \mathbb{1} \left\{ d_{\nu+\xi,s}^g(\mathbf{u}) < \widehat{d}_{\nu+\xi,s}^{g,lb}(\mathbf{u}) \right\} \\ &+ \frac{2}{\alpha} \left[ d_{\nu+\xi,s}^g(\mathbf{u}) - \widehat{d}_{\nu+\xi,s}^{g,ub}(\mathbf{u}) \right] \mathbb{1} \left\{ d_{\nu+\xi,s}^g(\mathbf{u}) > \widehat{d}_{\nu+\xi,s}^{g,ub}(\mathbf{u}) \right\}, \end{aligned}$$

where the level of significance is customarily set to be  $\alpha = 0.2$  or  $0.05$ . The interval score rewards a narrow prediction interval width if and only if  $100(1 - \alpha)\%$  of the holdout densities lie within the prediction interval.

For different ages and years in the testing set, the mean interval score is defined by

$$\bar{S}_\alpha(h) = \frac{1}{111 \times (17 - h)} \times \sum_{\xi=h}^{16} \sum_{u=1}^{111} S_{\alpha,\xi} \left[ \hat{d}_{v+\xi,s}^{g,lb}(u), \hat{d}_{v+\xi,s}^{g,ub}(u), d_{v+\xi,s}^g(u) \right].$$

Averaging over all forecast horizons, we obtain the overall mean interval score

$$\bar{S}_\alpha = \frac{1}{16} \sum_{h=1}^{16} \bar{S}_\alpha(h), \quad M[S_\alpha] = \text{median}[\bar{S}_\alpha(h)].$$

## 6.5 Comparison of interval forecast accuracy

In Table 2, averaged across 47 prefectures, we compare the interval forecast accuracy among the functional time-series models using the EVR criterion. From the summary statistics of the CPD and interval score at the level of significance  $\alpha = 0.2$ , the MFTS offers the smallest CPD value for the female data, while the UFTS and MLFTS offer the smallest CPD values for the male data. In terms of the interval scores, the UFTS and MFTS provide the smallest interval scores for the female data, while the FANOVA gives the smallest interval scores for the male data. In Appendix B, we also provide the results for  $K = 6$ .

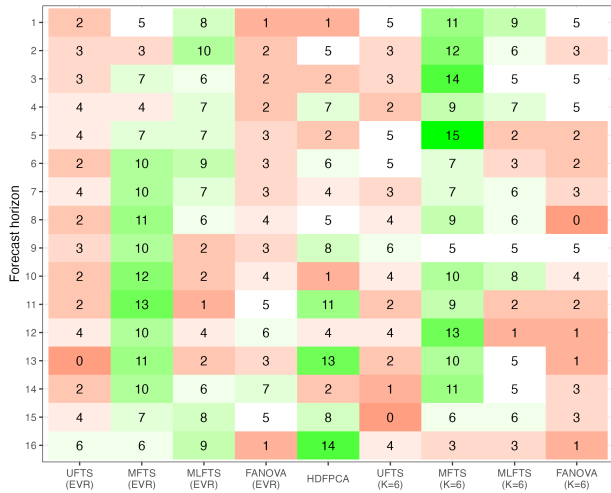
Table 2: Averaged across 47 prefectures, we evaluate and compare the interval forecast accuracy, as measured by the CPD and interval score, for the seven functional time-series models at the significance level  $\alpha = 0.2$ . The number of components is determined by the EVR criterion.

Metric	h	Female					Male				
		UFTS	MFTS	MLFTS	FANOVA	HDFPCA	UFTS	MFTS	MLFTS	FANOVA	HDFPCA
$\overline{CPD}_{0.2}$	1	0.061	0.080	0.047	0.075	0.077	0.060	0.100	0.043	0.079	0.067
	2	0.060	0.074	0.046	0.085	0.054	0.060	0.102	0.047	0.090	0.084
	3	0.058	0.068	0.050	0.096	0.091	0.058	0.105	0.055	0.094	0.086
	4	0.058	0.064	0.055	0.110	0.067	0.058	0.108	0.056	0.097	0.087
	5	0.053	0.056	0.057	0.113	0.094	0.053	0.101	0.056	0.096	0.085
	6	0.060	0.050	0.065	0.124	0.085	0.060	0.104	0.057	0.097	0.092
	7	0.061	0.048	0.069	0.125	0.084	0.061	0.097	0.057	0.091	0.094
	8	0.061	0.046	0.074	0.126	0.095	0.061	0.089	0.055	0.085	0.087
	9	0.068	0.047	0.081	0.128	0.072	0.068	0.083	0.062	0.076	0.084
	10	0.071	0.047	0.086	0.139	0.123	0.071	0.085	0.069	0.084	0.090
	11	0.078	0.049	0.093	0.145	0.059	0.078	0.087	0.075	0.085	0.084

Continued on next page

Metric	h	Female					Male				
		UFTS	MFTS	MLFTS	FANOVA	HDFPCA	UFTS	MFTS	MLFTS	FANOVA	HDFPCA
	12	0.075	0.053	0.092	0.146	0.126	0.075	0.083	0.078	0.085	0.089
	13	0.076	0.054	0.084	0.147	0.065	0.076	0.073	0.077	0.089	0.081
	14	0.073	0.068	0.087	0.147	0.100	0.073	0.078	0.084	0.095	0.099
	15	0.069	0.090	0.091	0.163	0.098	0.069	0.080	0.088	0.087	0.105
	16	0.062	0.098	0.093	0.178	0.062	0.062	0.077	0.081	0.085	0.088
	Mean	0.065	0.062	0.073	0.128	0.085	0.065	0.091	0.065	0.089	0.087
	Median	0.062	0.055	0.078	0.127	0.084	0.062	0.088	0.060	0.088	0.086
$\bar{S}_{0.2}$	1	268	256	433	287	325	256	279	218	258	248
	2	295	302	466	336	335	295	306	243	279	281
	3	317	347	494	389	402	317	332	265	293	306
	4	345	397	524	450	357	345	359	285	312	327
	5	368	445	551	508	457	368	379	300	321	344
	6	398	510	591	587	394	398	401	319	338	370
	7	420	583	618	672	547	420	415	339	354	394
	8	443	675	651	780	450	443	432	361	371	420
	9	465	763	688	885	633	465	446	386	386	441
	10	488	875	750	1033	492	488	473	409	398	484
	11	500	998	761	1191	775	500	491	439	421	513
	12	520	1159	862	1377	542	520	518	461	448	585
	13	527	1306	914	1572	1020	527	470	482	473	658
	14	563	1533	1058	1877	617	563	521	571	535	783
	15	627	1869	1225	2203	1432	627	588	700	621	924
	16	843	2151	1456	2526	848	843	807	991	865	1139
	Mean	481	481	784	1281	705	481	491	453	440	534
	Median	443	447	688	885	471	443	446	439	421	431

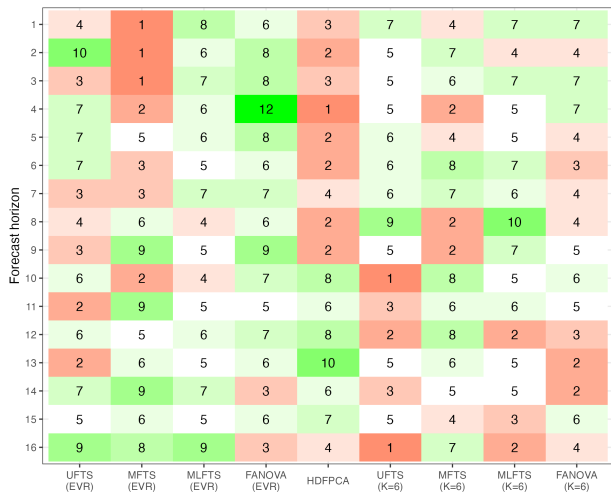
In Figure 7, we present two heatmaps comparing seven functional time-series models across 16 forecast horizons for both female and male testing data. For each horizon, we count how often each method produces the smallest interval forecast errors, as measured by the CPD and interval score. Based on the CPD results, we recommend the MFTS for the female data and the MLFTS for the male data, especially for  $K = 6$ . By examining the interval score results, we recommend the MFTS for shorter horizons and the HDFPCA for longer horizons in the female data. For the male data, the MFTS generally provides the smallest interval scores.



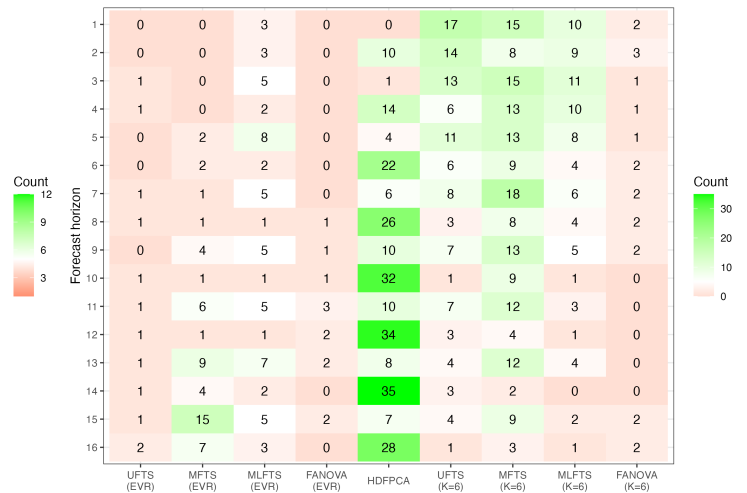
(a) CPD for females



(b) CPD for males



(c) Interval score for females



(d) Interval score for males

Figure 7: Heatmaps comparing the interval forecast accuracy at the significance level  $\alpha = 0.2$ , measured by the CPD and interval score, across seven functional time-series models and 16 forecast horizons for the female and male testing data. Since there are 47 prefectures, each row sums to 47. Methods that appear more than 5 times are shown in green, while those that appear fewer than 5 times are shown in red. If a method appears exactly five times, it is shown in white.

The interval forecast results at the significance level of  $\alpha = 0.05$  are available and can be viewed in a developed Shiny app at [https://cfjimenezv.shinyapps.io/Shiny\\_App\\_CDF/](https://cfjimenezv.shinyapps.io/Shiny_App_CDF/).

## 6.6 Forecasting Age-Specific Survival Probabilities and Life Expectancy

The enhanced forecast accuracy of subnational life-table death counts ( $\hat{d}_x$ ) enables precise estimation of key demographic indicators, such as the age-specific probability of dying ( $q_x$ ) and life expectancy ( $e_x$ ). These metrics are derived by constructing a complete life table from the forecasted

death counts ( $d_x$ ). Specifically, we apply the standard life table relationships using the `LifeTable` and `convertFx` functions from the `MortalityLaws` package (Pascariu, 2025) in `R`. The life table radix ( $l_0$ ) is set to 100,000 for all forecasted tables. For illustration, Figure 8 shows the forecasted distributions of deaths, probabilities of dying, and life expectancy for the prefecture Hokkaido for the years 2007 to 2023, based on data from 1975 to 2006.

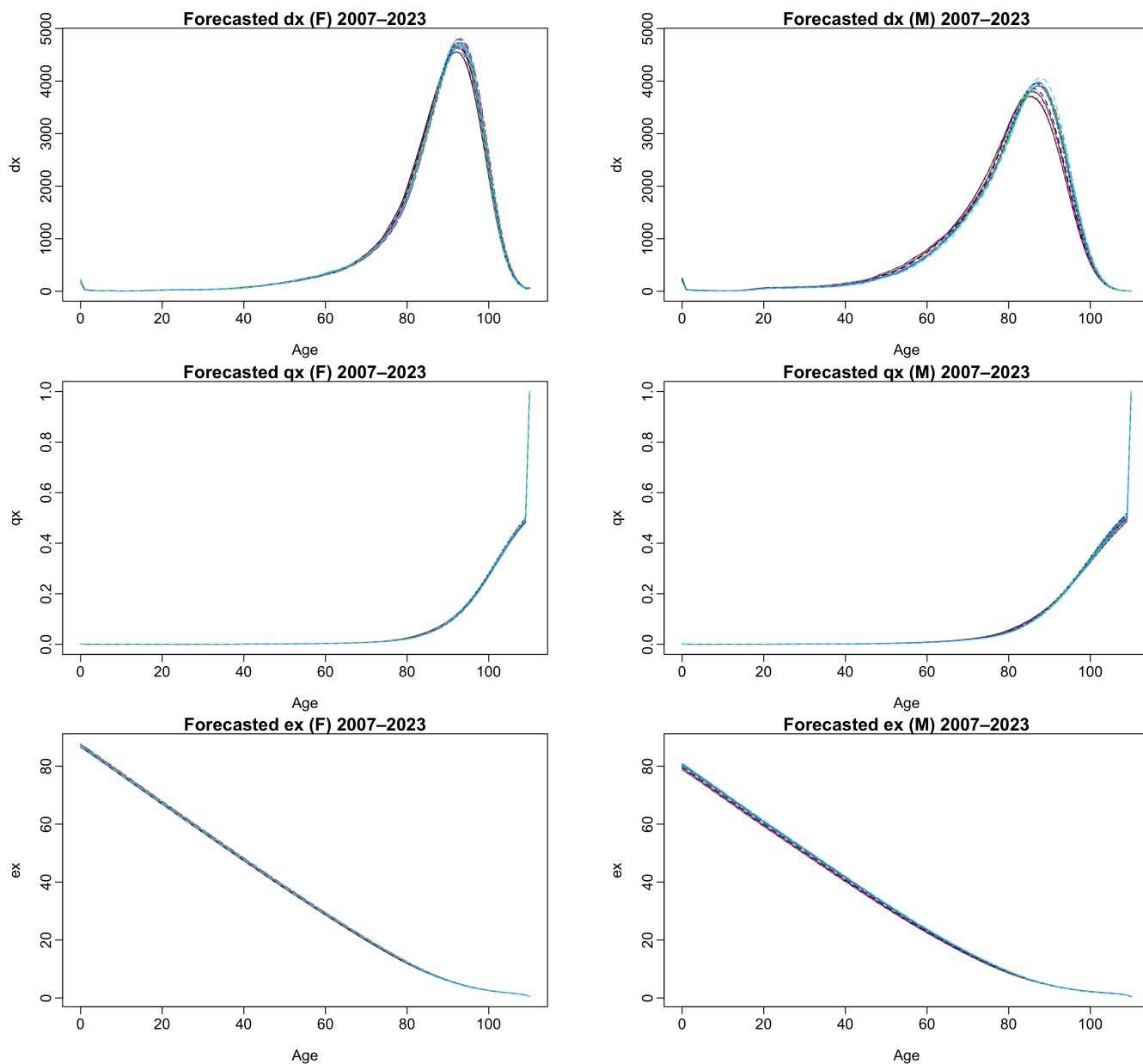


Figure 8: Forecasted life table metrics for Hokkaido, 2007–2023. Panels show age-specific deaths ( $d_x$ ), probability of dying ( $q_x$ ), and life expectancy ( $e_x$ ) for females (F) and males (M).

## 6.7 Model Diagnostics

We illustrate model diagnostics using the FANOVA residuals to assess the weak functional white noise assumption, focusing on stationarity and conditional heteroscedasticity. Stationarity was tested using the T-statistic-based method for functional time series (`T_stationary` in `ftsa` package in [R](#), [Hyndman and Shang, 2025](#)), separately for female and male residuals (matrices  $110 \times 49$  per prefecture). Conditional heteroscedasticity was assessed using the functional conditional heteroscedasticity test (`fCH_test` in `FTSgo` package in [R](#), [Rice et al., 2020](#)). Table 3 summarizes the p-values across the 47 prefectures. Since all p-values exceed 0.05, the residuals can be considered approximately stationary. Small p-values indicate some heteroscedasticity, but as our methods model the conditional mean, variance modeling is beyond the scope; functional GARCH-type models could be explored in future work.

Table 3: Summary of p-values from stationarity and conditional heteroscedasticity tests.

Gender	Min	1st Qu.	Median	Mean	3rd Qu.	Max
<u>Stationary test</u>						
Female	0.060	0.078	0.085	0.0853	0.091	0.108
Male	0.057	0.0705	0.079	0.0784	0.0855	0.099
<u>Conditional heteroscedasticity test</u>						
Female	0.0000	8.22e-15	1.64e-12	7.67e-04	2.58e-10	3.60e-02
Male	3.85e-13	3.35e-09	6.56e-06	1.61e-02	2.13e-04	4.88e-01

## 7 Conclusion

We present several graphical tools, namely image plots and cross-correlation plots, to visualize the differences and dependence in life-table death counts between each prefecture and Japan as a whole.

Via the CDF transformation, we consider a suite of functional time-series models to model and forecast the subnational age distribution of death counts for 47 Japanese prefectures. The CDF transformation is ideal for handling zero values in subnational data. Within the CDF transformation, we also present two general strategies for constructing pointwise prediction intervals.

By dividing the datasets into training and testing samples, we evaluate and compare the point and interval forecast accuracy among the functional time-series models. We confirm the

importance of joint modeling techniques, in which the MFTS, MLFTS, FANOVA, and HDFPCA models generally perform well on the aggregate level across 47 prefectures. We present a novel heatmap showing the frequency (of 47 prefectures), in which one method performs the best for each forecast horizon. Individual forecast errors for various horizons, obtained from all methods for each prefecture, are available in a developed shiny app at [https://cfjimenezv.shinyapps.io/Shiny\\_App\\_CDF/](https://cfjimenezv.shinyapps.io/Shiny_App_CDF/). The forecast life-table death counts are not only important to compute age-specific survival probability and life expectancy in demography, but they are also useful to determine annuity prices for various ages and maturities studied in [Shang and Haberman \(2020\)](#).

There are several ways in which the methodology can be extended, and we briefly list five. 1) The functional standard deviation in (8) was computed coordinate-wise. There is a range of functional depth that can be implemented to compute other variants of standard deviations. 2) Instead of symmetric prediction intervals, asymmetric ones can be considered, searching for two tuning parameters to adjust the lower and upper bounds. 3) Third, the data set was divided almost equally into training, validation, and testing samples. Other proportions may be possible, leading to a more accurate selection of the tuning parameter  $\xi_\alpha$  and more accurate interval forecasts. 4) We implemented a suite of functional time-series models for evaluation and comparison. Other time-series extrapolation models may also be considered, such as the robust functional principal component analysis by [Oguamalam et al. \(2025\)](#). It extends the Mahalanobis distance to Bayes spaces and introduces a regularized approach for improved principal component estimation in the presence of outliers. 5) We focus on modeling and forecasting the conditional mean. For modeling and forecasting conditional heteroskedasticity, the functional generalized autoregressive conditional heteroskedasticity (GARCh) model may be more adequate (see, e.g., [Aue et al., 2017](#); [Cerovecki et al., 2019](#); [Rice et al., 2020](#) and [2023](#); [Kearney et al., 2025](#)). Future work will be to incorporate the GARCh framework into some functional models considered.

## Supplementary Materials

1. **Code for the forecasting methods based on the CDF transformation.** The  code to produce point and interval forecasts from the different functional time-series models described in the paper. The  codes are available at the following repository: [https://github.com/cfjimenezv07/HDFTS\\_CDF/tree/main/Rcode](https://github.com/cfjimenezv07/HDFTS_CDF/tree/main/Rcode)

2. **Code for a shiny application.**The  code to produce a shiny user interface for the point and interval forecasts for the 47 Japanese prefectures. The  codes are available at the following repository: [https://github.com/cfjimenezv07/HDFTS\\_CDF/tree/main/Shiny\\_App\\_CDF](https://github.com/cfjimenezv07/HDFTS_CDF/tree/main/Shiny_App_CDF)

## Acknowledgment

This research was supported by the Australian Research Council Discovery Project (grant no. DP230102250) and Future Fellowship (grant no. FT240100338). We are grateful for the many insightful comments and suggestions from the seminar participants at the University of Melbourne and the University of New South Wales. The author is grateful to Dr Yang Yang from the University of Newcastle for assistance with the heatmaps.

# Appendix A: Point forecast accuracy when $K = 6$

In Table 4, averaged across 47 prefectures, we compare the point forecast accuracy among the functional time-series models, when the number of retained components is set to six as in Hyndman et al. (2013). Based on the summary statistics of the KLD and JSD, the MFTS provides the most accurate point forecasts for the female and male data.

Table 4: Averaged across 47 prefectures, we evaluate and compare the point forecast accuracy of the functional time-series models, measured by the KLD and JSD. The number of components is determined by setting  $K = 6$ .

Metric	h	Female				Male			
		UFTS	MFTS	MLFTS	FANOVA	UFTS	MFTS	MLFTS	FANOVA
KLD	1	0.004	0.004	0.004	0.006	0.003	0.003	0.003	0.004
	2	0.006	0.008	0.006	0.007	0.004	0.004	0.004	0.005
	3	0.008	0.009	0.008	0.008	0.005	0.005	0.005	0.005
	4	0.010	0.011	0.009	0.009	0.006	0.006	0.006	0.006
	5	0.012	0.013	0.010	0.011	0.006	0.007	0.006	0.007
	6	0.014	0.014	0.011	0.013	0.007	0.007	0.007	0.007
	7	0.017	0.016	0.013	0.015	0.008	0.008	0.008	0.008
	8	0.021	0.018	0.016	0.018	0.009	0.009	0.009	0.009
	9	0.026	0.021	0.019	0.022	0.010	0.010	0.010	0.011
	10	0.032	0.025	0.023	0.027	0.011	0.012	0.011	0.011
	11	0.039	0.029	0.027	0.033	0.012	0.013	0.013	0.013
	12	0.047	0.035	0.034	0.041	0.012	0.015	0.014	0.014
	13	0.058	0.042	0.040	0.048	0.013	0.017	0.015	0.015
	14	0.067	0.038	0.047	0.063	0.014	0.011	0.015	0.018
	15	0.088	0.053	0.067	0.083	0.014	0.014	0.020	0.023
	16	0.116	0.071	0.089	0.110	0.015	0.018	0.027	0.030
	17	0.151	0.085	0.106	0.125	0.015	0.020	0.031	0.033
Mean		0.042	0.029	0.031	0.038	0.010	0.011	0.012	0.013
Median		0.026	0.021	0.019	0.022	0.010	0.010	0.010	0.010

Continued on next page

Metric	h	Female				Male			
		UFTS	MFTS	MLFTS	FANOVA	UFTS	MFTS	MLFTS	FANOVA
JSD	1	0.032	0.034	0.033	0.037	0.027	0.026	0.026	0.031
	2	0.040	0.042	0.039	0.040	0.033	0.032	0.032	0.034
	3	0.044	0.046	0.043	0.043	0.035	0.034	0.034	0.036
	4	0.048	0.049	0.047	0.047	0.038	0.037	0.037	0.038
	5	0.052	0.053	0.050	0.051	0.040	0.039	0.039	0.040
	6	0.057	0.056	0.053	0.055	0.043	0.041	0.041	0.042
	7	0.062	0.059	0.057	0.059	0.045	0.043	0.043	0.044
	8	0.067	0.062	0.061	0.065	0.048	0.045	0.045	0.047
	9	0.074	0.066	0.066	0.070	0.051	0.047	0.048	0.049
	10	0.081	0.070	0.072	0.077	0.053	0.049	0.050	0.051
	11	0.090	0.076	0.079	0.087	0.055	0.051	0.052	0.054
	12	0.101	0.083	0.088	0.098	0.057	0.053	0.055	0.057
	13	0.115	0.090	0.098	0.109	0.059	0.056	0.058	0.060
	14	0.128	0.094	0.109	0.124	0.060	0.055	0.061	0.066
	15	0.149	0.111	0.130	0.144	0.061	0.060	0.069	0.074
	16	0.175	0.128	0.150	0.169	0.063	0.066	0.079	0.085
	17	0.201	0.137	0.164	0.181	0.063	0.069	0.085	0.089
	Mean	0.089	0.074	0.079	0.086	0.049	0.047	0.050	0.053
	Median	0.074	0.066	0.066	0.070	0.051	0.047	0.048	0.049

## Appendix B: Interval forecast accuracy when $K = 6$

In Table 5, averaged across 47 prefectures, we compare the interval forecast accuracy among the functional time-series models. From the summary statistics of the CPD and interval scores at the level of significance  $\alpha = 0.2$ , the MFTS offers the smallest CPD value for the female data, while the MLFTS offers the smallest CPD values for the male data. In terms of interval scores, the MFTS yields the smallest for the female data, while FANOVA yields the smallest for the male data.

Table 5: Averaged across 47 prefectures, we evaluate and compare the interval forecast accuracy, as measured by the CPD and interval score, among the functional time-series models at the level of significance  $\alpha = 0.2$ . The number of components is determined by setting  $K = 6$ . For either females or males, we highlight the method with the smallest overall CPD and interval scores.

Metric	h	Female				Male			
		UFTS	MFTS	MLFTS	FANOVA	UFTS	MFTS	MLFTS	FANOVA
CPD	1	0.052	0.042	0.045	0.058	0.054	0.049	0.046	0.051
	2	0.059	0.038	0.046	0.061	0.056	0.058	0.050	0.055
	3	0.066	0.041	0.057	0.068	0.055	0.060	0.052	0.057
	4	0.073	0.045	0.061	0.079	0.058	0.068	0.056	0.061
	5	0.072	0.045	0.059	0.084	0.058	0.070	0.054	0.062
	6	0.080	0.052	0.065	0.095	0.061	0.073	0.058	0.071
	7	0.084	0.049	0.066	0.097	0.059	0.073	0.054	0.069
	8	0.089	0.052	0.068	0.105	0.061	0.078	0.055	0.071
	9	0.090	0.054	0.073	0.106	0.070	0.077	0.060	0.067
	10	0.101	0.055	0.082	0.115	0.071	0.077	0.068	0.078
	11	0.108	0.056	0.087	0.128	0.075	0.084	0.076	0.118
	12	0.109	0.054	0.087	0.127	0.074	0.081	0.071	0.129
	13	0.113	0.054	0.076	0.127	0.071	0.075	0.075	0.128
	14	0.119	0.064	0.085	0.129	0.067	0.076	0.081	0.155
	15	0.120	0.091	0.093	0.135	0.065	0.080	0.084	0.156
	16	0.109	0.103	0.104	0.140	0.062	0.062	0.088	0.153
	Mean	0.089	0.056	0.073	0.112	0.065	0.071	0.063	0.094
	Median	0.090	0.053	0.067	0.108	0.062	0.073	0.058	0.071

Continued on next page

Metric	h	Female				Male			
		UFTS	MFTS	MLFTS	FANOVA	UFTS	MFTS	MLFTS	FANOVA
$\bar{S}_{0.2}$	1	233	253	234	248	239	221	208	225
	2	281	292	275	301	268	252	237	251
	3	326	325	310	352	294	278	261	275
	4	374	357	346	406	324	305	285	299
	5	421	388	376	460	348	327	304	321
	6	485	433	421	533	381	354	330	350
	7	558	480	468	614	403	372	353	369
	8	649	531	533	721	428	392	380	395
	9	734	587	602	825	450	408	404	418
	10	845	659	689	961	472	436	429	438
	11	969	756	800	1117	486	460	455	457
	12	1134	848	896	1305	513	485	471	487
	13	1283	872	999	1507	516	451	489	513
	14	1508	1035	1220	1804	552	504	572	573
	15	1834	1226	1466	2122	615	578	714	656
	16	2130	1463	1754	2410	840	797	942	903
	Mean	885	667	841	1376	484	465	502	460
	Median	734	587	689	1305	472	436	455	457

## Appendix C: Conformal prediction intervals

In machine learning, a popular methodology known as conformal prediction (Shafer and Vovk, 2008) is used to construct probabilistic forecasts calibrated on out-of-sample errors. From the absolute value of  $[\widehat{\varepsilon}_{1,s}^g(\mathbf{u}), \dots, \widehat{\varepsilon}_{M,s}^g(\mathbf{u})]$ , we compute its  $100(1 - \alpha)\%$  quantile for a level of significance  $\alpha$ , denoted by  $q_\alpha(\mathbf{u})$ . The prediction interval can be obtained as

$$\left[ \widehat{d}_{n+h|n,s}^g(\mathbf{u}) - q_\alpha(\mathbf{u}), \widehat{d}_{n+h|n,s}^g(\mathbf{u}) + q_\alpha(\mathbf{u}) \right],$$

where  $\widehat{d}_{n+h|n,s}^g(\mathbf{u})$  denotes the  $h$ -step-ahead point forecasts for the data in the testing set.

The conformal prediction approach performs well when the validation set has a reasonably large sample size (Dhillon et al., 2024). For smaller sample sets, we recommend using the standard deviation method described in Section 5. As shown in Table 6, the MLFTS achieves the lowest CPD values under the EVR criterion, whereas the MFTS provides the smallest CPD values for  $K = 6$  in the female dataset. For the male dataset, MLFTS is the preferred method. Regarding interval scores, MFTS attains the lowest values under the EVR criterion, while HDFPCA performs best for  $K = 6$  in the female data. For males, UFTS and FANOVA are favored under the EVR criterion, with MFTS performing best for  $K = 6$ .

Table 6: Averaged across 47 prefectures, we evaluate and compare the interval forecast accuracy, measured by the CPD and interval score, for the functional time-series models at the significance level  $\alpha = 0.2$ . The number of components is determined by the EVR criterion or  $K = 6$ ; for each, we highlight the method with the smallest overall CPD and interval score values.

Metric	Sex	h	EVR					K = 6			
			UFTS	MFTS	MLFTS	FANOVA	HDFPCA	UFTS	MFTS	MLFTS	FANOVA
CPD	F	1	0.090	0.109	0.063	0.090	0.102	0.067	0.056	0.054	0.067
		2	0.105	0.106	0.065	0.105	0.052	0.080	0.057	0.056	0.080
		3	0.120	0.099	0.066	0.120	0.118	0.091	0.057	0.062	0.091
		4	0.136	0.094	0.067	0.136	0.044	0.103	0.059	0.066	0.103
		5	0.141	0.084	0.062	0.141	0.130	0.109	0.060	0.064	0.109
		6	0.159	0.083	0.063	0.159	0.052	0.124	0.062	0.068	0.124
		7	0.161	0.080	0.071	0.161	0.133	0.133	0.064	0.073	0.133
		8	0.163	0.074	0.071	0.163	0.060	0.138	0.063	0.071	0.138
		9	0.172	0.077	0.075	0.172	0.130	0.147	0.068	0.077	0.147

Continued on next page

Metric	Sex	h	EVR				K = 6				
			UFTS	MFTS	MLFTS	FANOVA	HDFPCA	UFTS	MFTS	MLFTS	FANOVA
		10	0.183	0.080	0.081	0.183	0.054	0.161	0.075	0.084	0.161
		11	0.192	0.081	0.096	0.192	0.135	0.171	0.084	0.095	0.171
		12	0.199	0.095	0.106	0.199	0.055	0.178	0.095	0.108	0.178
		13	0.198	0.095	0.107	0.198	0.168	0.176	0.099	0.112	0.176
		14	0.221	0.115	0.129	0.221	0.082	0.188	0.115	0.132	0.188
		15	0.256	0.158	0.162	0.256	0.241	0.219	0.158	0.164	0.219
		16	0.299	0.190	0.186	0.299	0.138	0.256	0.191	0.201	0.256
		Mean	0.184	0.103	0.096	0.184	0.117	0.152	0.092	0.101	0.152
		Median	0.177	0.094	0.078	0.177	0.118	0.136	0.071	0.081	0.136
	M	1	0.094	0.122	0.062	0.094	0.090	0.058	0.064	0.063	0.058
		2	0.113	0.127	0.072	0.113	0.111	0.070	0.077	0.068	0.070
		3	0.119	0.130	0.076	0.119	0.115	0.076	0.083	0.070	0.076
		4	0.125	0.137	0.083	0.125	0.117	0.083	0.091	0.077	0.083
		5	0.123	0.137	0.087	0.123	0.122	0.090	0.098	0.080	0.090
		6	0.133	0.146	0.097	0.133	0.137	0.105	0.109	0.090	0.105
		7	0.134	0.139	0.099	0.134	0.142	0.111	0.107	0.090	0.111
		8	0.126	0.132	0.095	0.126	0.139	0.117	0.112	0.089	0.117
		9	0.116	0.127	0.093	0.116	0.139	0.118	0.110	0.087	0.118
		10	0.119	0.133	0.096	0.119	0.154	0.119	0.117	0.092	0.119
		11	0.114	0.129	0.100	0.114	0.160	0.118	0.118	0.099	0.118
		12	0.110	0.130	0.102	0.110	0.177	0.122	0.118	0.103	0.122
		13	0.100	0.121	0.093	0.100	0.172	0.121	0.114	0.091	0.121
		14	0.104	0.130	0.105	0.104	0.187	0.125	0.125	0.099	0.125
		15	0.115	0.143	0.118	0.115	0.196	0.133	0.136	0.114	0.133
		16	0.134	0.183	0.151	0.134	0.234	0.156	0.179	0.151	0.156
		Mean	0.120	0.135	0.097	0.120	0.142	0.104	0.107	0.092	0.104
		Median	0.119	0.133	0.096	0.119	0.138	0.118	0.113	0.091	0.118
$\bar{S}_{0.2}$	F	1	286	423	247	286	331	253	256	237	253
		2	338	459	285	338	323	308	297	280	308
		3	393	489	319	393	411	360	331	316	360
		4	457	521	354	457	349	419	366	353	419
		5	514	548	386	514	470	474	398	386	474

Continued on next page

Metric	Sex	h	EVR				K = 6				
			UFTS	MFTS	MLFTS	FANOVA	HDFPCA	UFTS	MFTS	MLFTS	FANOVA
		6	593	573	429	593	393	551	438	436	551
		7	671	601	477	671	549	632	481	486	632
		8	784	627	536	784	451	741	521	549	741
		9	897	660	600	897	624	855	570	617	855
		10	1050	715	676	1050	477	1001	633	707	1001
		11	1217	778	766	1217	735	1170	710	804	1170
		12	1396	877	862	1396	513	1356	802	908	1356
		13	1588	865	954	1588	968	1563	820	1003	1563
		14	1872	1015	1181	1872	570	1843	994	1237	1843
		15	2185	1199	1387	2185	1368	2153	1201	1469	2153
		16	2528	1343	1552	2528	619	2475	1358	1665	2475
		Mean	1092	731	740	1092	603	1095	630	742	1095
		Median	840	644	638	840	495	928	546	677	928
M		1	259	280	221	259	251	224	222	209	224
		2	281	309	247	281	286	249	253	238	249
		3	296	335	268	296	314	272	278	262	272
		4	312	359	287	312	334	291	303	284	291
		5	320	378	301	320	353	311	325	302	311
		6	337	399	319	337	383	337	350	325	337
		7	351	412	337	351	413	361	367	347	361
		8	366	424	359	366	438	385	383	372	385
		9	379	435	378	379	462	404	396	390	404
		10	394	457	397	394	504	420	420	412	420
		11	414	475	426	414	548	440	444	439	440
		12	440	507	445	440	626	468	472	456	468
		13	456	454	454	456	699	485	432	464	485
		14	500	498	545	500	839	528	481	551	528
		15	562	555	661	562	977	586	543	657	586
		16	609	600	744	609	1094	640	595	730	640
		Mean	393	419	396	393	516	395	387	414	395
		Median	372	418	378	372	450	400	375	381	400

# Appendix D: Model Confidence Set (MCS) Analysis

We performed a rigorous statistical comparison of the point forecast accuracy across all competing models using the **Model Confidence Set (MCS)** procedure (Hansen et al., 2011). The MCS procedure identifies a set of superior models,  $\mathcal{M}^*$ , where the null hypothesis of Equal Predictive Ability (EPA) cannot be rejected at a given significance level  $\alpha$ .

The analysis was based on the point forecast errors measured by the **Kullback-Leibler Divergence (KLD)** for nine Functional Time-Series (FTS) models over 17 forecast horizons ( $h = 1$  to  $h = 17$ ). The procedure was applied to the forecast errors for 47 Japanese prefectures separately for male and female mortality data. We used a significance level of  $\alpha = 0.10$ , a block-bootstrap approach with  $B = 2000$  resamples, and the  $T_{\max}$  statistic.

The heatmaps in Figure 9 visualize the results of the MCS procedure. In each cell, the count represents the number of prefectures (out of 47) for which the corresponding model was included in the statistically superior set  $\mathcal{M}^*$  at that horizon, demonstrating the robust predictive ability of the models across the regional series. For the female data, the **MLFTS** method consistently achieved statistical superiority across most prefectures at shorter horizons. Conversely, the **HDFPCA** method proved most robust at longer horizons. For the male dataset, the **MFTS** method was consistently included in the superior set  $\mathcal{M}^*$  for both short and long forecast horizons.

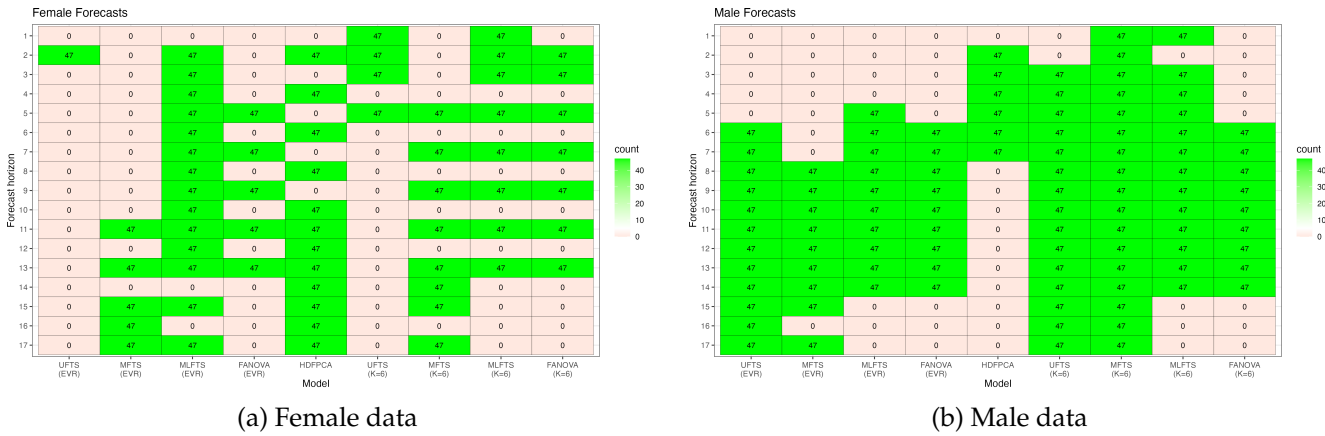


Figure 9: Heatmaps summarizing the results of the **Model Confidence Set (MCS)** procedure. The analysis compares the point forecast accuracy, measured by the Kullback-Leibler Divergence (KLD), across nine functional time-series models over 17 forecast horizons ( $h = 1$  to  $h = 17$ ) for both female and male mortality data. Each cell value indicates the number of the 47 prefectures for which the corresponding model was included in the superior set,  $\mathcal{M}^*$ , at that specific horizon (each row sums to 47). Cells are color-coded based on the count: **Green** highlights models included in the superior set for six or more prefectures ( $\geq 6$ ), **Red** for four or fewer prefectures ( $\leq 4$ ), and **White** for exactly five.

## References

- Aburto, J. and van Raalte, A. A. (2018), 'Lifespan dispersion in times of life expectancy fluctuation: the case of central and eastern Europe', *Demography* **55**, 2071–2096.
- Aitchison, J. (1986), *The Statistical Analysis of Compositional Data*, Monographs on Statistics and Applied Probability, Chapman & Hall.
- Aue, A., Horváth, L. and Pellatt, D. (2017), 'Functional generalized autoregressive conditional heteroskedasticity', *Journal of Time Series Analysis* **38**(1), 3–21.
- Bathia, N., Yao, Q. and Ziegelmann, F. (2010), 'Identifying the finite dimensionality of curve time series', *Annals of Statistics* **38**(6), 3352–3386.
- Bergeron-Boucher, M.-P., Simonacci, V., Oeppen, J. and Gallo, M. (2018), 'Coherent modeling and forecasting of mortality patterns for subpopulations using multiway analysis of compositions: An application to Canadian provinces and territories', *North American Actuarial Journal* **22**(1), 92–118.
- Booth, H. and Tickle, L. (2008), 'Mortality modelling and forecasting: A review of methods', *Annals of Actuarial Science* **3**(1-2), 3–43.
- Cairns, A. J. G., Blake, D. and Dowd, K. (2006), 'A two-factor model for stochastic mortality with parameter uncertainty: Theory and calibration', *Journal of Risk and Insurance* **73**(4), 687–718.
- Canudas-Romo, V. (2010), 'Three measures of longevity: Time trends and record values', *Demography* **47**(2), 299–312.
- Cattell, R. B. (1966), 'The screen test for the number of factors', *Multivariate Behavioral Research* **1**(2), 245–276.
- Cerovecki, C., Francq, C., Hörmann, S. and Zakoïan, J.-M. (2019), 'Functional GARCH models: the quasi-likelihood approach and its applications', *Journal of Econometrics* **209**(2), 353–375.
- Chang, J., Fang, Q., Qiao, X. and Yao, Q. (2025), 'On the modeling and prediction of high-dimensional functional time series', *Journal of the American Statistical Association: Theory and Methods* **in press**.

- Cheung, S. L. K., Robine, J.-M., Tu, E. J.-C. and Caselli, G. (2005), 'Three dimensions of the survival curve: Horizontalization, verticalization, and longevity extension', *Demography* **42**(2), 243–258.
- Coulmas, F. (2007), *Population Decline and Ageing in Japan – the Social Consequences*, Routledge, New York.
- Cuesta-Albertos, J. A. and Febrero-Bande, M. (2010), 'A simple multiway ANOVA for functional data', *Test* **19**(3), 537–557.
- d'Albis, H., Esso, L. J. and i Arolas, H. P. (2014), 'Persistent differences in mortality patterns across industrialized countries', *PLoS One* **9**(9), e106176.
- Debón, A., Chaves, L., Haberman, S. and Villa, F. (2017), 'Characterization of between-group inequality of longevity in EU countries', *Insurance: Mathematics and Economics* **75**, 151–165.
- Denuit, M., Devolder, P. and Goderniaux, A.-C. (2007), 'Securitization of longevity risk: Pricing survivor bonds with Wang transform in the Lee-Carter framework', *The Journal of Risk and Insurance* **74**(1), 87–113.
- Dhillon, G. S., Deligiannidis, G. and Rainforth, T. (2024), On the expected size of conformal prediction sets, in 'Proceedings of the 27th International Conference on Artificial Intelligence and Statistics (AISTATS)', Vol. 238, Valencia, Spain.
- Edwards, R. D. and Tuljapurkar, S. (2005), 'Inequality in life spans and a new perspective on mortality convergence across industrialized countries', *Population and Development Review* **31**(4), 645–674.
- Fuglede, B. and Topsoe, F. (2004), Jensen-Shannon divergence and Hilbert space embedding, in 'Proceedings of International Symposium on Information Theory', IEEE, Chicago. URL: <https://ieeexplore.ieee.org/document/1365067>.
- Gao, Y., Shang, H. L. and Yang, Y. (2019), 'High-dimensional functional time series forecasting: An application to age-specific mortality rates', *Journal of Multivariate Analysis* **170**, 232–243.
- Gneiting, T. and Raftery, A. E. (2007), 'Strictly proper scoring rules, prediction, and estimation', *Journal of the American Statistical Association: Review Article* **102**(477), 359–378.
- Guo, S., Qiao, X. and Wang, Q. (2025), 'Factor modelling for high-dimensional functional time series', *Journal of Business & Economic Statistics* **in press**.

- Haberman, S. and Renshaw, A. (2011), 'A comparative study of parametric mortality projection models', *Insurance: Mathematics and Economics* **48**(1), 35–55.
- Hall, P. and Vial, C. (2006), 'Assessing the finite dimensionality of functional data', *Journal of the Royal Statistical Society: Series B* **68**(4), 689–705.
- Hallin, M., Nisol, G. and Tavakoli, S. (2023), 'Factor models for high-dimensional functional time series I: Representation results', *Journal of Time Series Analysis* **44**(5-6), 578–600.
- Hansen, P. R., Lunde, A. and Nason, J. M. (2011), 'The model confidence set', *Econometrica* **79**(2), 453–497.
- Hyndman, R. J. and Athanasopoulos, G. (2021), *Forecasting: Principles and Practice*, OTexts.
- Hyndman, R. J., Booth, H. and Yasmeen, F. (2013), 'Coherent mortality forecasting: the product-ratio method with functional time series models', *Demography* **50**(1), 261–283.
- Hyndman, R. J. and Khandakar, Y. (2008), 'Automatic time series forecasting: the forecast package for R', *Journal of Statistical Software* **27**(3), 1–22.
- Hyndman, R. J., Koehler, A., Ord, K. and Snyder, R. (2008), *Forecasting with exponential smoothing: the state-space approach*, Springer, Berlin; London.
- Hyndman, R. and Shang, H. L. (2025), *ftsa: Functional Time Series Analysis*. R package version 6.7.
- Japanese Mortality Database (2025), *National Institute of Population and Social Security Research*. Available at <https://www.ipss.go.jp/p-toukei/JMD/index-en.asp> (data downloaded on September 18, 2024).
- Jiménez-Varón, C. F., Sun, Y. and Shang, H. L. (2024), 'Forecasting high-dimensional functional time series: Application to sub-national age-specific mortality', *Journal of Computational and Graphical Statistics* **33**(4), 1160–1174.
- Jiménez-Varón, C. F., Sun, Y. and Shang, H. L. (2025), 'Forecasting density-valued functional panel data', *Australian & New Zealand Journal of Statistics* **67**(3), 401–415.
- Kearney, F., Shang, H. L. and Zhao, Y. (2025), Intraday FX volatility-curve forecasting with functional GARCH approaches, Technical report, arXiv. URL: <https://arxiv.org/abs/2311.18477>.

- Kneip, A. and Utikal, K. J. (2001), 'Inference for density families using functional principal component analysis', *Journal of the American Statistical Association: Theory and Methods* **96**(454), 519–532.
- Kokoszka, P., Rice, G. and Shang, H. L. (2017), 'Inference for the autocovariance of a functional time series under conditional heteroscedasticity', *Journal of Multivariate Analysis* **162**, 32–50.
- Kullback, S. and Leibler, R. A. (1951), 'On information and sufficiency', *The Annals of Mathematical Statistics* **22**(1), 79–86.
- Lee, R. D. and Carter, L. R. (1992), 'Modeling and forecasting U.S. mortality', *Journal of the American Statistical Association: Applications & Case Studies* **87**(419), 659–671.
- Leng, C., Li, D., Shang, H. L. and Xia, Y. (2026), 'Covariance function estimation for high-dimensional functional time series with dual factor structures', *Journal of Business & Economic Statistics* **in press**.
- Li, D., Li, R. and Shang, H. L. (2024), 'Detection and estimation of structural breaks in high-dimensional functional time series', *The Annals of Statistics* **52**(4), 1716–1740.
- Li, D., Robinson, P. M. and Shang, H. L. (2020), 'Long-range dependent curve time series', *Journal of the American Statistical Association: Theory and Methods* **115**(530), 957–971.
- Li, N. and Lee, R. (2005), 'Coherent mortality forecasts for a group of populations: An extension of the Lee–Carter method', *Demography* **42**, 575–594.
- Lu, Q., Hanewald, K., Villegas, A. and Wang, X. (2020), Subnational old-age mortality modeling: Accounting for underreporting in a Bayesian framework, Technical report, SSRN.  
**URL:** [https://papers.ssrn.com/sol3/papers.cfm?abstract\\_id=3687266](https://papers.ssrn.com/sol3/papers.cfm?abstract_id=3687266)
- Lu, Q., Hanewald, K. and Wang, X. (2021), 'Subnational mortality modelling: A Bayesian hierarchical model with common factors', *Risks* **9**(11), 203.
- Mayhew, L. and Smith, D. (2013), 'A new method of projecting populations based on trends in life expectancy and survival', *Population Studies* **67**(2), 157–170.
- Mestre, G., Portela, J., Rice, G., Roque, A. M. S. and Alonso, E. (2021), 'Functional time series model identification and diagnosis by means of auto- and partial autocorrelation analysis', *Computational Statistics and Data Analysis* **155**, 107108.

- Morris, J. S. and Carroll, R. J. (2006), 'Wavelet-based functional mixed models', *Journal of the Royal Statistical Society: Series B* **68**(2), 179–199.
- Nakahara, S. and Ichikawa, M. (2013), 'Mortality in the 2011 Tsunami in Japan', *Journal of Epidemiology* **23**(1), 70–73.
- Oeppen, J. (2008), Coherent forecasting of multiple-decrement life tables: A test using Japanese cause of death data, in 'European Population Conference', Barcelona, Spain. Available online at <https://epc2008.eaps.nl/papers/80611>.
- Oguamalam, J., Filzmoser, P., Hron, K., Menafoglio, A. and Radojčić, U. (2025), Robust functional PCA for density data, Technical report, arXiv. URL: <https://arxiv.org/pdf/2412.19004>.
- Okamoto, S., Yamada, A., Kobayashi, E. and Liang, J. (2025), 'Socioeconomic inequity in access to medical and long-term care among older people', *International Journal for Equity in Health* **24**, Article number 28.
- Pascariu, M. D. (2025), *MortalityLaws: Parametric Mortality Models, Life Tables and HMD*. R package version 2.1.3. URL: <https://CRAN.R-project.org/package=MortalityLaws>.
- Petersen, A., Zhang, C. and Kokoszka, P. (2022), 'Modeling probability density functions as data objects', *Econometrics and Statistics* **21**, 159–178.
- Poskitt, D. S. and Sengarapillai, A. (2013), 'Description length and dimensionality reduction in functional data analysis', *Computational Statistics and Data Analysis* **58**(2), 98–113.
- Rice, G., Wirjanto, T. and Zhao, Y. (2020), 'Tests for conditional heteroscedasticity of functional data', *Journal of Time Series Analysis* **41**(6), 733–758.
- Rice, G., Wirjanto, T. and Zhao, Y. (2023), 'Exploring volatility of crude oil intraday return curves: A functional GARCH-X model', *Journal of Commodity Markets* **32**, 100361.
- Shafer, G. and Vovk, V. (2008), 'A tutorial on conformal prediction', *Journal of Machine Learning Research* **9**, 371–421.
- Shang, H. L. (2025), 'Forecasting a time series of Lorenz curves: One-way functional analysis of variance', *Journal of Applied Statistics* **52**(15), 2924–2940.

- Shang, H. L. and Haberman, S. (2020), 'Forecasting age distribution of death counts: An application to annuity pricing', *Annals of Actuarial Science* **14**, 150–169.
- Shang, H. L. and Haberman, S. (2025a), 'Constructing prediction intervals for the age distribution of deaths', *Scandinavian Actuarial Journal* **in press**.
- Shang, H. L. and Haberman, S. (2025b), 'Forecasting age distribution of deaths: Cumulative distribution function transformation', *Insurance: Mathematics and Economics* **122**, 249–261.
- Shang, H. L. and Haberman, S. (2025c), 'Forecasting age distribution of life-table death counts via  $\alpha$ -transformation', *Scandinavian Actuarial Journal* **2025**(4), 387–403.
- Shannon, C. E. (1948), 'A mathematical theory of communication', *Bell System Technical Journal* **27**(3), 379–423.
- Shibata, R. (1981), 'An optimal selection of regression variables', *Biometrika* **68**(1), 45–54.
- Tanaka, H., Mackenbach, J. P. and Kobayashi, Y. (2023), 'Estimation of socioeconomic inequalities in mortality in Japan using national census-linked longitudinal mortality data', *Journal of Epidemiology* **33**(5), 246–255.
- Tang, C., Shang, H. L. and Yang, Y. (2022), 'Clustering and forecasting multiple functional time series', *The Annals of Applied Statistics* **16**, 2523–2553.
- Tavakoli, S., Nisol, G. and Hallin, M. (2023), 'Factor models for high-dimensional functional time series II: Estimation and forecasting', *Journal of Time Series Analysis* **44**(5-6), 601–621.
- Tu, I.-P., Chen, H. and Chen, X. (2009), 'An eigenvector variability plot', *Statistica Sinica* **19**(4), 1741–1754.
- van Raalte, A. A. and Caswell, H. (2013), 'Perturbation analysis of indices of lifespan variability', *Demography* **50**(5), 1615–1640.
- Wang, S., Jank, W. and Shmueli, G. (2008), 'Explaining and forecasting online auction prices and their dynamics using functional data analysis', *Journal of Business and Economic Statistics* **26**(2), 144–160.
- Wilmoth, J. R. and Horiuchi, S. (1999), 'Rectangularization revisited: Variability of age at death within human populations', *Demography* **36**(4), 475–495.

Zhou, Z. and Dette, H. (2023), 'Statistical inference for high-dimensional panel functional time series', *Journal of the Royal Statistical Society: Series B* **85**(2), 523–549.

Zivot, E. and Wang, J. (2006), *Modeling Financial Time Series with S-PLUS*, Springer, New York.